Block Lanczos and many-body theory: Application to the one-particle Green's function

H.-G. Weikert, H.-D. Meyer, and L. S. Cederbaum
Theoretische Chemie, Physikalisch-Chemisches Institut, Universität Heidelberg, Im Neuenheimer Feld 253, 69120 Heidelberg, Germany

F. Tarantelli
Dipartimento di Chimica, Università di Perugia, Via Elce di Sotto 8, I-06123 Perugia, Italy

(Received 28 September 1995; accepted 29 January 1996)

The importance of the block or band Lanczos method for many-body Green's function calculations of atomic and molecular systems is discussed. The usual computation schemes for determining the Green's function involve the diagonalization of Hermitian secular matrices. Considerable numerical difficulties arise, on the one hand, from the size of these matrices and, on the other hand, from the large number of eigenvalues and eigenvectors which often need to be computed in practice. In the case of the one-particle Green's function it is shown how the computational effort of the diagonalization process can be substantially reduced using block Lanczos. The proposed procedure which consists of a block Lanczos ''prediagonalization'' and a subsequent diagonalization of the resulting smaller secular matrices quite naturally exploits the specific structure of the secular problems encountered. Its computational performance is demonstrated in a model application to the benzene molecule. The calculation of the complete valence-shell ionization spectra of the systems BeF_4^{2-}, BeF_3^-, and BeF_2 is devised as a further application of the method in the particular case where the treatment of the full secular problem is computationally prohibitively expensive. [S0021-9606(96)01817-8]

I. INTRODUCTION

In the framework of many-body theory the Green's function formalism[1–4] constitutes a powerful and elegant theoretical tool for investigating properties and excitation processes in many-particle systems. The Green's function provides direct access to important physical quantities as, for example, ionization energies and spectral intensities by the one-particle Green's function without the need to resort to separate (approximate) solutions of the Schrödinger equation for the (initial) ground state and the (final) ionic states. Hereby the method accounts from the outset for a balanced consideration of both the ground and ionic correlation which is difficult within conventional wave function approaches such as the configuration interaction (CI) method. Another inherent advantage of the Green's function approach, being essential for the treatment of larger systems is the occurence of ''size-consistent'' approximation schemes which have the correct scaling behavior with respect to the number of electrons.

The essential numerical elements associated with the computation of the Green's function involve the evaluation of matrix elements and the diagonalization of Hermitian matrices defined in the space of a special class of ionic configurations. One source of problems one has to cope with in realistic applications results from the size of the configuration space. Depending on the size of the molecule, the orbital basis set, and the approximation scheme used, the configuration space can become extremely large preventing the determination of the relevant eigenvalues and eigenvectors from the corresponding secular matrix with reasonable expense. Another drawback arises from the large number of eigenstates which often need to be computed in order to ensure a conclusive assignment of the observed structures in the experimental spectrum.

Though large-scale eigenelement computations represent a standard task in computational quantum chemistry and physics, the specific problem to be solved often permits some reasonable simplifications. A particular interesting situation is encountered in the case of the one-particle Green's function. Here, one may resort to the well-known Dyson equation relating the one-particle Green's function to the so-called self-energy which is an effective energy-dependent one-particle potential. When solving the Dyson equation one usually makes use of the well-established equivalence of this equation to the evaluation of the eigenvalues and eigenvectors of Hermitian secular matrices possessing a specific structure. The secular matrices to be diagonalized consist of three submatrices (blocks): the one-particle block, the $(N+1)$-particle block, and the $(N-1)$-particle block. The sizes of the configuration spaces defining these submatrices are, however, very different. Whereas the one-particle block corresponds to the space of single-particle and single-hole configurations and is small, the $(N-1)$-particle block and, in particular, the $(N+1)$-particle block, which are associated with physical excitations of $N-1$ and $N+1$ particles, respectively, are usually of high dimension. The fact that the $(N+1)$-particle and $(N-1)$-particle blocks can be treated independently and that these blocks are energetically far apart from each other is of crucial importance. Therefore, provided that one is only interested in the eigenvalues and eigenvector components corresponding to the ionization energies and spectral intensities of a molecule, one may ''replace'' the

 0021-9606/96/104(18)/7122/17/$10.00

usually *very large* $(N+1)$-particle block, which is expected to have only minor influence on the desired cationic solutions, by a *much smaller* matrix which approximates the $(N+1)$-particle block well in the region of ionization.

An obvious way of truncating the $(N+1)$-particle block is to perform a selection in the configuration space, e.g., by including the most important configurations in the calculations and excluding the others. This may, however, largely affect the accuracy of the final results. Another and apparently more promising way of approximating the $(N+1)$-particle block is to rely on projection methods. These techniques consist of generating an increasing subspace onto which the $(N+1)$-particle block—or, in general, a large symmetric or Hermitian matrix **H**—is restricted. The choice of basis vectors spanning the subspace is, however, crucial and depends on the specific problem under consideration. The probably most prominent projection method which has found widespread application is the single-vector (simple) Lanczos algorithm.[5–7] Using the Lanczos recurrence, the algorithm iteratively builds an orthonormal basis from the Krylov subspace, i.e., from the sequence of iterates $\{q_1,\mathbf{H}q_1,...,\mathbf{H}^{j-1}q_1\}$, where q_1 is an initial vector called the starting vector. In this basis spanned by the Lanczos vectors the representation of the matrix **H** is particularly simple. It reduces to a tridiagonal matrix which is easy to diagonalize or to invert.

The natural extension of the simple scheme is the block or band Lanczos method.[6–8] In exact arithmetic both variants are equivalent. Though being computationally more demanding than the single-vector Lanczos method, the block Lanczos method is, as we shall see, particularly well adapted to the present purposes. The major (formal) differences with the simple scheme are that the block algorithm generates a *set* of orthonormal vectors at once in time instead of *one* as does the simple scheme and that the matrices resulting from projection are now no longer tridiagonal but block tridiagonal or banded. Originally the block Lanczos algorithm was conceived to identify the multiplicity of degenerate eigenvalues for which the single-vector algorithm does not account for. However, as mentioned, owing to its greater complexity the block Lanczos method has been rarely used. It is just recently that its efficiency has been demonstrated in calculating matrix elements of a resolvent.[9,10]

It is one of the inherent advantages of both the simple and block Lanczos methods that they permit the computation of a few of the eigenvalues and eigenvectors of a matrix **H** without the need to perform a complete (similarity) transformation of **H**. This is due to the iterative nature of the process, providing at each iteration a tridiagonal or block tridiagonal matrix. From the numerical side the simple structure of these matrices is also important. Indeed, many applications use the Lanczos algorithm as a diagonalization method for large matrices. Another insight into the convergence behavior of the Lanczos method results from its close relationship to the methods of moments.[11,12] It is well-known that the moments of a matrix **H** are intimately related to the matrix elements of the tridiagonal or block tridiagonal representation of **H** with respect to the Lanczos basis. This implies that the Lanczos spectra converge in a global sense towards the exact eigenspectrum of **H**. In general, the first few moments usually already allow a reasonable description of the global features of **H**'s spectrum (position, width, shape, etc.), whereas the higher moments account for more refined details of the spectrum leaving, however, its crude structure unchanged. Because of this significant feature, the block Lanczos method offers new possibilities for applications to many-body Green's functions.

The objective of this article is to analyze the capability of the block Lanczos method for many-body Green's function calculations. In the particular case of the one-particle Green's function we shall demonstrate how, due to the specific structure of the secular matrices encountered, the block Lanczos method is quite naturally applied allowing for an effective reduction of the size of the diagonalization problem. In Sec. II we briefly outline the theory of the one-particle Green's function and the particular approximation scheme employed here. In Sec. III we survey two of the probably most widely used diagonalization methods for large matrices in quantum chemistry and physics: the Lanczos and the Davidson algorithms. The new proposed procedure for the numerical calculation of the one-particle Green's function is then described in Sec. IV. The discussions in Secs. V and VI are devoted to provide model applications demonstrating the performance of the proposed method. Finally, concluding remarks are presented in Sec. VII.

II. THE ONE-PARTICLE GREEN'S FUNCTION AND ITS EVALUATION

The one-particle Green's function $\mathbf{G}(\omega)$ is the simplest member in the hierarchy of Green's functions. Consider an N-particle system (atom or molecule) with a nondegenerate (closed-shell) ground state $|\psi_0^N\rangle$ and energy E_0^N. In a basis spanned by the discrete set of one-particle states $|\phi_p\rangle$—usually chosen as the ground state Hartree–Fock (HF) orbitals—the matrix elements of $\mathbf{G}(\omega)$ in energy representation are defined as[1,4]

$$G_{pq}(\omega)=\langle\psi_0^N|c_p(\omega+E_0^N-\hat{H}+i\eta)^{-1}c_q^\dagger|\psi_0^N\rangle + \langle\psi_0^N|c_q^\dagger(\omega-E_0^N+\hat{H}-i\eta)^{-1}c_p|\psi_0^N\rangle. \tag{1}$$

Here, $c_p^\dagger(c_p)$ labels the creation (annihilation) operator for an electron in the one-particle state $|\phi_p\rangle$ obeying the usual anticommutation relations, $\hat{H}$ is the (full) electronic Hamiltonian of the system, and η is a positive infinitesimal introduced to ensure the convergence of the Fourier transform between the time and energy representations of $\mathbf{G}(\omega)$. The physical content of the one-particle Green's function becomes more apparent in its spectral representation[1,4]

$$G_{pq}(\omega)=\sum_n \frac{\langle\psi_0^N|c_p|\psi_n^{N+1}\rangle\langle\psi_n^{N+1}|c_q^\dagger|\psi_0^N\rangle}{\omega+E_0^N-E_n^{N+1}+i\eta} + \sum_n \frac{\langle\psi_0^N|c_q^\dagger|\psi_n^{N-1}\rangle\langle\psi_n^{N-1}|c_p|\psi_0^N\rangle}{\omega+E_n^{N-1}-E_0^N-i\eta} \tag{2}$$

which readily results from Eq. (1) by inserting complete sets of $(N\pm1)$-particle eigenstates $|\psi_n^{N\pm1}\rangle$ of $\hat{H}$ with energies

$E_n^{N\pm1}$. The first (advanced) and second (retarded) parts of $\mathbf{G}(\omega)$ bear important information on the electron attachment (or scattering) and ionization processes, respectively. The (vertical-electronic) ionization energies

$$I_n = E_n^{N-1} - E_0^N \tag{3}$$

and electron affinities

$$A_n = E_0^N - E_n^{N+1} \tag{4}$$

are derived from the location of the poles of $\mathbf{G}(\omega)$ in the upper and lower half, respectively, of the complex energy plane. The residue corresponding to a pole n is obtained as the product of the transition (or spectroscopic) amplitudes

$$x_p^{(n)} = \begin{cases} \langle \psi_0^N | c_p | \psi_n^{N+1} \rangle & n \in \{N+1\} \\ \\ \langle \psi_n^{N-1} | c_p | \psi_0^N \rangle & n \in \{N-1\} \end{cases} . \tag{5}$$

The amplitudes $x_p^{(n)}$ are closely related to the spectral intensities of the experiment. Consider the case of an ionization experiment where the kinetic energy E_ϵ of the ejected electron is sufficiently high (''sudden limit''). The intensity with which a final ionic state n in the spectrum emerges is given by[13]

$$P^{(n)}(E_\epsilon) = \sum_\epsilon \left| \sum_p \tau_{\epsilon p} x_p^{(n)} \right|^2 \delta(E_\epsilon + I_n - \omega_0). \tag{6}$$

Here, $\tau_{\epsilon p}$ denotes the dipole matrix element for the (bound) one-particle state $|\phi_p\rangle$ and the continuum (scattering) one-particle state $|\psi_\epsilon\rangle$ and ω_0 is the energy of the incident photon. Often only one orbital p has appreciable contribution to $P^{(n)}(E_\epsilon)$. In this case Eq. (6) simplifies to

$$P^{(n)}(E_\epsilon) = P_{pn} \sum_\epsilon |\tau_{\epsilon p}|^2 \delta(E_\epsilon + I_n - \omega_0), \tag{7}$$

where

$$P_{pn} = |x_p^{(n)}|^2. \tag{8}$$

The quantity P_{pn} is called *pole strength or spectroscopic factor* and provides a measure for the relative spectral intensities of the ionic states n associated with the orbital p. For a more thorough discussion of the intensity problem we refer to Refs. 14 and 15.

To evaluate the one-particle Green's function $\mathbf{G}(\omega)$ one usually starts from the Dyson equation[1,4]

$$\mathbf{G}(\omega) = \mathbf{G}^0(\omega) + \mathbf{G}^0(\omega)\mathbf{\Sigma}(\omega)\mathbf{G}(\omega) \tag{9}$$

relating $\mathbf{G}(\omega)$ to the so-called self-energy $\mathbf{\Sigma}(\omega)$. The free Green's function $\mathbf{G}^0(\omega)$ appearing in Eq. (9) is defined with respect to the noninteracting HF particles. Its matrix elements in energy space read

$$G_{pq}^0(\omega) = \delta_{pq} \left(\frac{n_p}{\omega - \epsilon_p - i\eta} + \frac{\overline{n_p}}{\omega - \epsilon_p + i\eta} \right), \tag{10}$$

where ϵ_p are the HF orbital energies and $n_p = 1 - \overline{n_p}$ denote the HF ground state occupation numbers. As for $\mathbf{G}(\omega)$ there exists a direct perturbation expansion for $\mathbf{\Sigma}(\omega)$ in terms of the famous Feynman diagrams. The self-energy $\mathbf{\Sigma}(\omega)$ consists of a static (energy-independent) part $\mathbf{\Sigma}(\infty)$ discussed further below (see Sec. IV B) and a dynamic (energy-dependent) part $\mathbf{M}(\omega)$:

$$\mathbf{\Sigma}(\omega) = \mathbf{\Sigma}(\infty) + \mathbf{M}(\omega). \tag{11}$$

The dynamic self-energy is further split into two parts according to

$$\mathbf{M}(\omega) = \mathbf{M}^{\mathrm{I}}(\omega) + \mathbf{M}^{\mathrm{II}}(\omega) \tag{12}$$

each possessing a spectral representation[16–18]

$$M_{pq}^{\mathrm{I,II}}(\omega) = \sum_{\mu \in \{N\pm1\}} \frac{m_p^{(\mu)} m_q^{(\mu)*}}{\omega - \omega_\mu + i\eta\sigma_{\mathrm{I,II}}} \tag{13}$$

similar to that for the one-particle Green's function. Depending on the sign of σ, the poles ω_μ are located either in the lower ($\sigma_{\mathrm{I}} = +1$) or the upper half ($\sigma_{\mathrm{II}} = -1$) of the complex energy plane. The residue corresponding to a pole μ is given as the product of the coupling (Dyson) amplitudes $m_p^{(\mu)}$. The decomposition of the dynamic self-energy into the parts $\mathbf{M}^{\mathrm{I}}(\omega)$ and $\mathbf{M}^{\mathrm{II}}(\omega)$ implies that each of these parts can be calculated independently, for instance, from their respective diagrammatic perturbation expansions. There are *no mixed* terms between the parts I and II. Physically these parts are associated with excitations of the $(N\pm1)$-particle systems.

Using the relations (10)–(13), the solution of the Dyson equation can be cast as an eigenvalue problem of a Hermitian matrix.[19] In practical applications one, of course, uses an approximation of the self-energy and hence of this Hermitian matrix. Various approximation schemes have been proposed to evaluate the self-energy and Green's functions in general. An important class of approximation schemes are the diagrammatical methods. Here, one makes use of the Feynman diagrams to represent the perturbation series of the Green's function or propagator under consideration. Among the diagrammatical methods the algebraic diagrammatic construction (ADC)[20–23] has proven to be of particular success for the treatment of finite electronic systems. This scheme, which provides access to the entire energy scale of the valence-shell ionization regime, reformulates the diagrammatic perturbation expansion for the Green's function in a simple algebraic form representing infinite partial summations of certain types of Feynman diagrams. The nth-order scheme, ADC(n), is complete through finite order n perturbation theory, i.e., it includes all Feynman diagrams up to nth order as well as higher order contributions in an appropriate manner. The method is quite general and applies to any Green's function or single component of it. The present applications comprise the particle–hole (polarization) propagator,[20] the self-energy of the one-particle Green's function,[21] the particle–particle propagator,[22,23] and, more recently, the three-particle propagator.[24]

To be specific we concentrate here without loss of generality on the ADC scheme. The ADC is a generalization of the special (diagonal) representation (13). It is based on the observation that the dynamic self-energy can be represented in the algebraic form

$$M_{pq}(\omega)=\mathbf{U}_p^{\dagger}(\omega\mathbf{1}-\mathbf{K}-\mathbf{C})^{-1}\mathbf{U}_q. \tag{14}$$

Here, the superscripts I and II have been dropped. The matrix $\mathbf{K}$ introduced in Eq. (14) is diagonal and collects the zero-order (HF) excitation energies, $\mathbf{C}$ denotes a constant (energy-independent) Hermitian matrix referred to as the modified (effective) interaction matrix, and $\mathbf{U}_p$ is a constant vector of modified (effective) coupling amplitudes. The configuration space defining these quantities comprises all physical ($N\pm1$)-particle excitations with respect to the basis of the N-particle ground state HF orbitals excluding, however, the single-particle ($1p$) and single-hole ($1h$) configurations. In the usual classification scheme the electronic configurations are denoted as two-particle one-hole ($2p1h$), three-particle two-hole ($3p2h$),..., configurations (for block I) and as two-hole one-particle ($2h1p$), three-hole two-particle ($3h2p$),..., configurations (for block II).

In the ADC scheme both the vectors $\mathbf{U}_p$ and the matrix $\mathbf{C}$ possess perturbation expansions

$$\mathbf{U}_p=\mathbf{U}_p^{(1)}+\mathbf{U}_p^{(2)}\ldots, \tag{15}$$

$$\mathbf{C}=\mathbf{C}^{(1)}+\mathbf{C}^{(2)}\ldots, \tag{16}$$

each series beginning in first order. Upon expanding the matrix $(\omega\mathbf{1}-\mathbf{K}-\mathbf{C})^{-1}$ into powers of $(\omega\mathbf{1}-\mathbf{K})^{-1}\mathbf{C}$ and inserting the expansions (15) and (16) into Eq. (14) one arrives at

$$\begin{aligned}M_{pq}(\omega)=&\mathbf{U}_p^{(1)\dagger}(\omega\mathbf{1}-\mathbf{K})^{-1}\mathbf{U}_q^{(1)}+\mathbf{U}_p^{(1)\dagger}(\omega\mathbf{1}-\mathbf{K})^{-1}\mathbf{C}^{(1)}\\&\times(\omega\mathbf{1}-\mathbf{K})^{-1}\mathbf{U}_q^{(1)}+\mathbf{U}_p^{(2)\dagger}(\omega\mathbf{1}-\mathbf{K})^{-1}\mathbf{U}_q^{(1)}\\&+\mathbf{U}_p^{(1)\dagger}(\omega\mathbf{1}-\mathbf{K})^{-1}\mathbf{U}_q^{(2)}+\ldots,\end{aligned} \tag{17}$$

where all terms up to third order are shown. The matrix elements of $\mathbf{C}$ and $\mathbf{U}_p$ are obtained by comparing the ADC expansion of Eq. (17) with the original diagrammatic perturbation series for the dynamic self-energy parts $\mathbf{M}^{\mathrm{I}}(\omega)$ and $\mathbf{M}^{\mathrm{II}}(\omega)$. By construction, the ADC(n) scheme sums up all diagrams completely through nth order and includes, moreover, infinitely many diagrams of higher orders. In the ADC(2) approximation, also referred to as two-particle–hole Tamm–Dancoff approximation ($2ph$-TDA), one employs the first-order expansions for the elements of $\mathbf{C}$ and $\mathbf{U}_p$. The ADC(3) approximation (extended $2ph$-TDA) is obtained by replacing the first-order expansions for the coupling amplitudes $\mathbf{U}_p$ with the second-order expansions. The explicit expressions of the ADC equations for $\mathbf{C}$ and $\mathbf{U}_p$ up to fourth order are given in Ref. 21.

It is worthwhile mentioning that the ADC scheme combines perturbation theory (for the N-electron ground state) and matrix diagonalization (variational principle) which has no analogue within the conventional wave function picture. An essential property of the ADC scheme, being important in numerical applications, concerns the size of the configuration space. As is well-known (see, e.g., Ref. 21), the configuration space required by the nth-order scheme, ADC(n), is substantially smaller than that of comparable configuration interaction (CI) expansions for calculating the energies and transition moments consistent through nth order. The *explicit* ADC(n) space increases with each even order n. Hence, for $n=2$ and 3 the space is spanned by the $2p1h$ and $2h1p$ configurations and for $n=4$ and 5, in addition, by the $3p2h$ and $3h2p$ configurations of $N+1$ and $N-1$ particles, respectively. On the other hand, multiple products of two-particle interaction (Coulomb) matrix elements appear in the expressions of the ADC equations. This is in contrast to the familiar CI treatment where the Coulomb matrix elements enter the CI expansions exclusively in linear form, however, to the price of much larger configuration spaces.

Once the vectors $\mathbf{U}_p$ and the matrix $\mathbf{C}$ have been determined the Dyson equation (9) can be cast into the following eigenvalue problem:

$$\mathbf{BX}'=\mathbf{X}'\mathbf{E},\quad \mathbf{X}'\mathbf{X}'^{\dagger}=\mathbf{1}, \tag{18}$$

where

$$\mathbf{B}=\begin{pmatrix}\boldsymbol{\epsilon}+\boldsymbol{\Sigma}(\infty) & (\mathbf{U}^{\mathrm{I}})^{\dagger} & (\mathbf{U}^{\mathrm{II}})^{\dagger}\\ \mathbf{U}^{\mathrm{I}} & \mathbf{K}^{\mathrm{I}}+\mathbf{C}^{\mathrm{I}} & \mathbf{0}\\ \mathbf{U}^{\mathrm{II}} & \mathbf{0} & \mathbf{K}^{\mathrm{II}}+\mathbf{C}^{\mathrm{II}}\end{pmatrix}. \tag{19}$$

Here, $\boldsymbol{\epsilon}$ denotes the diagonal matrix of HF orbital energies and $\mathbf{U}$ is the matrix of (column) vectors $\mathbf{U}_p$ representing the coupling of the one-particle block $\boldsymbol{\epsilon}+\boldsymbol{\Sigma}(\infty)$ and the matrices $\mathbf{K}+\mathbf{C}$ of the blocks I and II. The one-particle Green's function $\mathbf{G}(\omega)$ is obtained as the upper left block of the inverse of the matrix $\omega\mathbf{1}-\mathbf{B}$,

$$G_{pq}(\omega)=[\omega\mathbf{1}-\mathbf{B}]^{-1}_{pq}, \tag{20}$$

or, explicitly,

$$G_{pq}(\omega)=\sum_n \frac{x_p^{(n)}x_q^{(n)*}}{\omega-e_n}, \tag{21}$$

where the poles and residue amplitudes of $\mathbf{G}(\omega)$ derive from the eigenvalues $e_n=E_{nn}$ and the corresponding eigenvector components $x_p^{(n)}=X'_{pn}$, respectively, of the matrix $\mathbf{B}$.

Instead of this one-step ''direct'' diagonalization of $\mathbf{B}$ one may alternatively first diagonalize the ADC matrices $\mathbf{K}+\mathbf{C}$ independently for the blocks I and II:

$$(\mathbf{K}+\mathbf{C})\mathbf{Y}=\mathbf{Y}\boldsymbol{\Omega},\quad \mathbf{YY}^{\dagger}=\mathbf{1}. \tag{22}$$

In a subsequent step the Dyson equation is then solved via the diagonalization problem

$$\mathbf{AX}=\mathbf{XE},\quad \mathbf{XX}^{\dagger}=\mathbf{1}, \tag{23}$$

where

$$\mathbf{A}=\begin{pmatrix}\boldsymbol{\epsilon}+\boldsymbol{\Sigma}(\infty) & \mathbf{m}^{\mathrm{I}} & \mathbf{m}^{\mathrm{II}}\\ (\mathbf{m}^{\mathrm{I}})^{\dagger} & \boldsymbol{\Omega}^{\mathrm{I}} & \mathbf{0}\\ (\mathbf{m}^{\mathrm{II}})^{\dagger} & \mathbf{0} & \boldsymbol{\Omega}^{\mathrm{II}}\end{pmatrix}. \tag{24}$$

The subblocks $\boldsymbol{\Omega}^{\mathrm{I,II}}$ and $\mathbf{m}^{\mathrm{I,II}}$ of the matrix $\mathbf{A}$ are the diagonal matrices of eigenvalues ω_μ of Eq. (22) representing the poles of the dynamic self-energy parts $\mathbf{M}^{\mathrm{I,II}}(\omega)$ and the matrices of coupling (Dyson) amplitudes $m_p^{(\mu)}$ [see Eqs. (12) and (13)], respectively, the latter being obtained according to

$$m_p^{(\mu)}=\mathbf{U}_p^{\dagger}Y^{(\mu)} \tag{25}$$

as the scalar product of $\mathbf{U}_p$ and the eigenvector $Y^{(\mu)}$ of Eq. (22) associated with the μth eigenvalue. The one-particle Green's function $\mathbf{G}(\omega)$ is again given in the form of Eqs. (20) and (21).

III. DIAGONALIZATION METHODS FOR LARGE MATRICES

The diagonalization of large symmetric or Hermitian matrices $\mathbf{H}$ is a key problem in computational quantum chemistry and physics. The usual way of calculating the eigenspectrum of $\mathbf{H}$ is to transform the matrix $\mathbf{H}$ into a tridiagonal one which is easy to diagonalize or to invert. However, standard diagonalization procedures such as the Givens and Householder methods[25] are not suitable for large matrices, since they have storage demands that depend on the square of the order N of the matrix $\mathbf{H}$ and require a number of arithmetic operations that scale as the cube of the matrix order (N^3 algorithms). Therefore, alternative procedures have to be considered in order to compute at least part of the eigenspectrum of $\mathbf{H}$.

In this section we review two diagonalization methods which have found widespread application: the Lanczos and the Davidson algorithms. Particular emphasis is placed on their respective block extensions. Both methods can be applied to calculate the eigenspectrum of a given matrix $\mathbf{H}$. However, while the Lanczos method is particularly suited to problems where information on the whole eigenspectrum of the matrix $\mathbf{H}$ is desired, the Davidson method offers the potential of a more efficient computation of a few selected (targeted) eigenvalues and eigenvectors of $\mathbf{H}$.

The common idea of both the Lanczos and the Davidson algorithms is to iteratively generate from an initial vector, called the starting vector, an increasing basis of orthonormal vectors

$$\mathbf{Q}^{(j)}=(q_1,q_2,\ldots,q_j) \tag{26}$$

onto which the matrix $\mathbf{H}$ is projected:

$$\mathbf{S}=\mathbf{Q}^{(j)\dagger}\mathbf{H}\mathbf{Q}^{(j)}. \tag{27}$$

The eigenvalues of the $j\times j$ matrix $\mathbf{S}$, called the Ritzvalues, represent approximations to certain eigenvalues of the matrix $\mathbf{H}$. Accompanying approximate eigenvectors $Y_\mu^{(j)}$ of $\mathbf{H}$, called the Ritzvectors, are obtained via the transformation

$$Y_\mu^{(j)}=\mathbf{Q}^{(j)}X_\mu^{(j)}, \tag{28}$$

where $X_\mu^{(j)}$ denotes the eigenvector corresponding to the μth eigenvalue of $\mathbf{S}$. Formally, the Lanczos and Davidson methods differ from each other essentially in the choice of the expansion vectors q_i.

A. Block or band Lanczos algorithm

The single-vector (simple) Lanczos algorithm is described in several textbooks and articles (see, e.g., Refs. 5–7 for textbooks and Refs. 26–33 for applications and further developments). The classical Lanczos procedure was originally conceived to reduce the eigenvalue problem of a large symmetric matrix to that of the simpler Lanczos matrices. The simple Lanczos method realizes an orthogonal projection process onto the Krylov space, i.e., the space spanned by the sequence of iterates $\{q_1,\mathbf{H}q_1,\ldots,\mathbf{H}^{j-1}q_1\}$. Starting with an initial (orthonormalized) vector q_1 with a nonzero projection on each eigenvector of $\mathbf{H}$, the algorithm builds an orthonormal basis $\{q_1,q_2,\ldots,q_j\}$ from the Krylov space, leading to a tridiagonal matrix $\mathbf{T}^{(j)}$. The computation of both the Lanczos vectors q_i and the matrix elements of $\mathbf{T}^{(j)}$ is extremely cheap. This is based upon the three-term recurrence

$$T_{i,i+1}q_{i+1}=\mathbf{H}q_i-T_{ii}q_i-T_{i,i-1}q_{i-1}, \tag{29}$$

where

$$T_{ii}=q_i^\dagger\mathbf{H}q_i \quad \text{and} \quad T_{i,i+1}=T_{i+1,i}^*=q_{i+1}^\dagger\mathbf{H}q_i \tag{30}$$

denote the diagonal and offdiagonal entries, respectively, of the tridiagonal matrix $\mathbf{T}^{(j)}$ and, by definition, $T_{i0}=0$ and $q_0=0$. Convergence is best[6] for the extreme eigenelements of $\mathbf{T}^{(j)}$ which usually contain most of the desired information.

It is an essential drawback of the simple Lanczos algorithm that it does not account for multiplicities of the eigenvalues which it computes. This suggests to consider a block or band extension of the simple scheme. The block algorithm[6,7] is readily derived from the simple algorithm by replacing the Lanczos vectors q_i and the numbers T_{ij} in the recursion (29) by their corresponding matrix analogues, yielding a block tridiagonal representation of the matrix $\mathbf{H}$. Alternatively, one may resort to a band formulation of the algorithm.[8] In the context of exact arithmetic both variants are equivalent. In the following, we consider the band algorithm rather than its block analog but shall use both names synonymously.

The band Lanczos algorithm starts by supplying n orthonormal vectors $q_1,q_2,\ldots,q_n$. The recursion relation then reads

$$T_{i,i+n}q_{i+n}=\mathbf{H}q_i-\sum_{j=i-n}^{i+n-1}T_{ij}q_j, \tag{31}$$

where

$$T_{ij}=T_{ji}^*=q_i^\dagger\mathbf{H}q_j \tag{32}$$

and, by definition, $T_{ij}=0$ and $q_i=0$, if $j\leqslant 0$. In the basis $\mathbf{Q}^{(j)}$ spanned by the Lanczos vectors q_i generated the projection of the matrix $\mathbf{H}$ becomes banded the bandwidth of which is $2n+1$:

$$\mathbf{T}^{(j)}=\mathbf{Q}^{(j)\dagger}\mathbf{H}\mathbf{Q}^{(j)}$$

$$=\begin{pmatrix} T_{11} & T_{12} & \cdots & T_{1n} & & & & \\ T_{21} & T_{22} & \ddots & & \ddots & & & \\ \vdots & \ddots & \ddots & \ddots & & \ddots & & \\ T_{n1} & & \ddots & \ddots & \ddots & & T_{*j} & \\ & \ddots & & \ddots & \ddots & \ddots & \vdots & \\ & & \ddots & & \ddots & \ddots & \vdots & \\ & & & T_{j*} & \cdots & \cdots & T_{jj} & \end{pmatrix}. \tag{33}$$

In practice, the algorithm is performed as

$$
\begin{aligned}
&r:=\mathbf{H}q_i-\sum_{j=i-n}^{i-1} T_{ij}q_j\\
&\text{For}\quad j=i,\ldots,i+n-1\\
&T_{ij}:=r^{\dagger}q_j\\
&r:=r-T_{ij}q_j\\
&\text{end do}\\
&T_{i,i+n}:=\|r\|\\
&q_{i+n}:=r/T_{i,i+n}\,.
\end{aligned}
\tag{34}
$$

Here, $\|\cdot\|$ denotes the Euclidean norm. Note that the single-vector algorithm is readily recovered for $n=1$. The band Lanczos algorithm iterates each starting vector at least

$$J=[j/n] \tag{35}$$

times, where $[m]$ is the entire part of m and J denotes the number of block iterations. We mention that in the block version the iteration number j is restricted to be an integer multiple of n.

As with the simple Lanczos method, the block Lanczos method is particularly attractive for the diagonalization of large matrices. This is due to the following reasons. First, the matrix $\mathbf{H}$ only enters the recurrence relation in form of the matrix×vector terms $\mathbf{H}q_i$. Second, only the $2n$ most recently generated Lanczos vectors q_i are required in order to compute the next n Lanczos vectors. Third, the block tridiagonal or band matrices generated by the block or band Lanczos method are easy to diagonalize. This allows, in principle, the computation of all the eigenvalues *and* eigenvectors of the matrix $\mathbf{H}$. In practice, however, the efficiency of the method diminishes due to numerical instabilities. As the iteration proceeds, the Lanczos vectors tend to lose their orthogonality and the process starts to produce copies of already converged eigenvalues. These instabilities can be remedied either by a complete or selective (partial) reorthonormalization of the Lanczos vectors (see, e.g., Ref. 6) which is, however, computationally expensive.

There is a certain range of problems in theoretical physics and chemistry where one is not interested in the individual eigenvalues and eigenvectors of the matrix $\mathbf{H}$, but rather in the global feature of its eigenspectrum. As an example we mention the evaluation of matrix elements of operator functions, $\langle\psi_p|F(\hat{H})|\psi_q\rangle$, to which the block Lanczos method is ideally adapted.[10] Here, $|\psi_p\rangle$ denote some reference vectors. To be more specific we recall from Ref. 10 the following remarkable properties of the block Lanczos method:

$$(\mathbf{H}^{(j)})^k|q_m\rangle=\mathbf{H}^k|q_m\rangle \quad \text{for } 1\leqslant m\leqslant n,\quad 0\leqslant k\leqslant J-1 \tag{36}$$

and

$$
\begin{aligned}
&\langle q_{m'}|(\mathbf{H}^{(j)})^k|q_m\rangle\\
&\qquad=\begin{cases}
\text{for } 1\leqslant m,m'\leqslant n & \\
\langle q_{m'}|\mathbf{H}^k|q_m\rangle & \text{for } 0\leqslant k\leqslant 2J-1,\ J=\text{odd}\\
\text{for } 0\leqslant k\leqslant 2J-2,\ J=\text{even} &
\end{cases}
\end{aligned}
\tag{37}
$$

where the matrix

$$\mathbf{H}^{(j)}=\mathbf{Q}^{(j)}\mathbf{Q}^{(j)\dagger}\mathbf{H}\mathbf{Q}^{(j)}\mathbf{Q}^{(j)\dagger}=\mathbf{Q}^{(j)}\mathbf{T}^{(j)}\mathbf{Q}^{(j)\dagger} \tag{38}$$

denotes the projection of $\mathbf{H}$ onto the j-dimensional Lanczos space. These relations state that the first $2J-2$ or $2J-1$ moments of $\mathbf{H}^{(j)}$ with respect to the starting vectors are exact. Moreover, it can be shown that there exists no approximation of rank j which gives more exact moments than the block Lanczos approximation $\mathbf{H}^{(j)}$. Hence, the block Lanczos method provides access to the desired global convergence in the sense of Eqs. (36) and (37). It permits, in particular, the fast computation of the elements $\langle\psi_p|F(\hat{H})|\psi_q\rangle$ of any operator function $F(\hat{H})$ provided that this function is analytic in a circle which contains the eigenvalues of $\mathbf{H}$. As has been demonstrated in Ref. 10 for the case of the resolvent $F(\mathbf{H})=(\omega-\mathbf{H})^{-1}$ (here, $\mathbf{H}$ is a matrix representation of the operator $\hat{H}$) one observes an exponential convergence of $\langle\psi_p|F(\hat{H}^{(j)})|\psi_q\rangle$ towards $\langle\psi_p|F(\hat{H})|\psi_q\rangle$ with the number of block iterations J times the ''distance'' from the spectrum, i.e., with $J\cdot\min_\mu|E_\mu-\omega|$, where E_μ denote the eigenvalues of $\mathbf{H}$. This convergence is extremely fast if ω is far apart, i.e., below or above, from the spectrum. It is this outstanding global convergence property of the block Lanczos method which establishes its relevance for applications within the many-body framework.

B. Block Davidson algorithm

The Davidson algorithm[34] has a long tradition in computational *ab initio* quantum chemistry. It is a standard method for finding the lowest eigenvalues and eigenvectors of large CI matrices.[35] A block extension of this method[36,37] has successfully been applied to the computation of valence-shell double ionization (Auger) spectra using the Green's function method.[38] For a recent discussion of the Davidson method see Ref. 39. Here, we give a brief account of the block Davidson method as implemented in the present calculations which is an extension of Ref. 37.

The idea behind the Davidson procedure is best illustrated by starting with a simple perturbation theory analysis. Upon partitioning a given matrix $\mathbf{H}$ as

$$\mathbf{H}=\mathbf{H}_0+\mathbf{H}_\mathrm{I} \tag{39}$$

into a dominant part $\mathbf{H}_0$—usually, and for the sake of simplicity, $\mathbf{H}_0=\mathrm{diag}(\mathbf{H})$ [diagonal preconditioning]—and a ''perturbation'' $\mathbf{H}_\mathrm{I}$, one is immediately led to a simple iteration scheme for improving a given trial eigenvector $c^{(j)}$ by a correction vector

$$\xi^{(j)}=[E^{(j)}\mathbf{1}-\mathbf{H}_0]^{-1}r^{(j)}. \tag{40}$$

Here, j denotes the iteration number, $E^{(j)}$ is the Rayleigh quotient for $c^{(j)}$ defined by

$$E^{(j)}=c^{(j)\dagger}\mathbf{H}c^{(j)}/c^{(j)\dagger}c^{(j)} \tag{41}$$

and

$$r^{(j)}=(\mathbf{H}-E^{(j)}\mathbf{1})c^{(j)} \tag{42}$$

its residual vector. The iteration scheme implied by Eq. (40) can also be regarded as the first-order approximation to the

method of ''coordinate relaxation''[40] applied simultaneously along all coordinates. While this simple scheme exhibits generally poor convergence properties,[34] the idea behind the Davidson method is not just to add the correction vector $\xi^{(j)}$ to $c^{(j)}$, but rather to progressively collect the correction vectors $\{\xi^{(j)}\}$ to form a basis set (after suitable reorthonormalization) in which the trial eigenvector is expanded. Thus the Davidson method also represents one particular implementation among the subspace iteration techniques. In general, we then write the trial eigenvector at cycle j as

$$c^{(j)}=\mathbf{Q}^{(j)}v^{(j)}, \tag{43}$$

where $\mathbf{Q}^{(j)}$ is a matrix of (column) orthonormal basis vectors and $v^{(j)}$ is the vector of expansion coefficients. For ease of notation we shall now drop the superscript indicating iteration number.

The matrix $\mathbf{Q}$ comprises any initial set of starting basis vectors—e.g., chosen to span a subspace of interest or the presumed dominant character of the sought eigenvectors—plus the successively collected and reorthonormalized correction vectors computed via Eq. (40). Specific criteria of choice for the initial $\mathbf{Q}$ used in the present work will be discussed later. At each iteration the vector v is chosen as usual by making the Rayleigh quotient stationary in the subspace spanned by $\mathbf{Q}$, i.e., among the eigenvectors of the matrix $\mathbf{S}=\mathbf{Q}^{\dagger}\mathbf{Z}$, with $\mathbf{Z}=\mathbf{HQ}$. This choice may easily be driven by any one of a number of criteria such as: eigenvalue minimization or restriction in a given range; eigenvector overlap maximization from one iteration to the next; magnitude of the eigenvector projection onto a specific subspace, and so on.

When more than one eigensolution of the matrix $\mathbf{H}$ is sought, two possible alternative procedures may obviously be conceived: The desired eigenpairs can be iterated independently and in succession, one after convergence of the other; or they can be refined simultaneously, at each cycle one new basis vector being computed and added to $\mathbf{Q}$ for each sought solution. The latter approach (''block Davidson'') is clearly characterized by a faster growth rate of the basis set, but this disadvantage is usually more than compensated by a much better convergence rate, especially in dense regions of the spectrum of $\mathbf{H}$. In addition, the block Davidson approach affords greater computational efficiency, in that a number of vector operations are naturally replaced by their matrix analogues, and the matrix $\mathbf{H}$ needs be computed or read from slow storage fewer times.

In practice, the algorithm is outlined in the following major steps:

(1) Supply and store an initial basis set matrix $\mathbf{Q}$ spanning a chosen subspace selected by some criteria. The basis vectors can also be chosen to be a subset of Ritzvectors from a previous run, thus implementing a restart mechanism. Form and store $\mathbf{Z}=\mathbf{HQ}$ and $\mathbf{S}=\mathbf{Q}^{\dagger}\mathbf{Z}$.

(2) Diagonalize $\mathbf{S}$ and select the desired eigenpairs (E_i,v_i) which have not yet converged. The vectors $\{v_i\}$ are collected in a matrix $\mathbf{V}$.

(3) Compute the residual matrix
$$\mathbf{R}=\mathbf{ZV}-\mathbf{QVE}, \tag{44}$$
where $\mathbf{E}=\mathrm{diag}(E_i)$.

(4) Test for convergence of the eigenvectors (e.g., $\|r_i\|$ less than a prescribed threshold). For each computed vector, store $c_i=\mathbf{Q}v_i$. For each unconverged vector, compute $\xi_i=[E_i\mathbf{1}-\mathbf{H}_0]^{-1}r_i$.

(5) Orthogonalize the $\{\xi_i\}$ vectors among themselves and to $\mathbf{Q}$. Normalize to form the new basis vectors $\mathbf{Q}'$, which are appended to the $\mathbf{Q}$ file.

(6) Form $\mathbf{Z}'=\mathbf{HQ}'$ and append it to the $\mathbf{Z}$ file.

(7) Update the $\mathbf{S}$ matrix by computing $\mathbf{Q}'^{\dagger}\mathbf{Z}'$ and $\mathbf{Q}^{\dagger}\mathbf{Z}'$.

(8) Repeat from step (2) until all selected vectors have converged or the subspace size has reached the allowed maximum.

The procedure lends itself to being automatically and dynamically implemented in virtually any amount of available fast storage, provided this is large enough to hold a few vectors. The vectors $\{z_i\}$ and $\{q_i\}$ (matrices $\mathbf{Z}$ and $\mathbf{Q}$) are kept on disk and read in groups of adjustable size. All the necessary matrix operations are also easily stripmined if needed to generate and handle only a suitable subset of correction and converged vectors at once. The amount of available storage also determines the maximum reachable size of the $\mathbf{Q}$ subspace, but, as outlined in step (1) above, the whole procedure is straightforwardly restartable by jumping from any step to step (1) and replacing the initial set of basis vectors with an appropriate subset of the current trial (and converged) eigenvectors. In this way the procedure automatically monitors and controls the growth rate of the subspace size and, if required, can truncate the subspace according to available resources.

In practice, convergence is usually achieved within a few iterations, in particular when the matrix $\mathbf{H}$ is diagonally dominant. As in the block Lanczos method, the time-consuming step is the formation of the $\mathbf{Z}$ matrix [step (6)]. On the other hand, the expansion vectors in the Davidson method do not obey a three-term recursion and the $\mathbf{S}$ matrix is not tridiagonal. This restricts the algorithm to handling generally smaller subspaces and to applications where a smaller number of selected roots are sought.

IV. NUMERICAL COMPUTATION OF THE ONE-PARTICLE GREEN'S FUNCTION

As has been discussed in Sec. II the determination of the one-particle Green's function requires

(i) The solution of the Dyson equation in form of either the ''direct'' diagonalization of the secular matrix $\mathbf{B}$ or the two-step procedure which comprises the diagonalization of the matrices $(\mathbf{K}+\mathbf{C})^{\mathrm{I,II}}$ according to Eq. (22) and the subsequent diagonalization of the matrix $\mathbf{A}$ specified in Eq. (24);

(ii) The evaluation of the static self-energy matrix $\mathbf{\Sigma}(\infty)$.

Matrices possessing a structure as does $\mathbf{A}$ are called ''arrow'' matrices. They are characterized to consist of a submatrix of small dimension and of a large diagonal ''tail''

coupled to the former submatrix via coupling matrices. A very efficient and numerically stable procedure for the diagonalization of **A** that takes advantage of its particular ''arrow type'' structure has been described in Refs. 41 and 42. This method, referred to as the pole search algorithm (PSA), enables the calculation of *all* the eigenvalues and eigenvectors of **A** within a certain range of its eigenspectrum. The drawback of the method, however, is that it requires the separate *full* diagonalization of the matrices $(\mathbf{K}+\mathbf{C})^{\mathrm{I,II}}$ prior to the construction of **A**. This clearly represents a formidable obstacle in view of the usually very large configuration spaces which define $(\mathbf{K}+\mathbf{C})^{\mathrm{I,II}}$. Therefore, in order to reduce the size of these matrices various possibilities such as, e.g., the truncation of the one-particle (orbital) space and/or the selection of important configurations have been considered. Nevertheless, in particular for the treatment of larger systems and basis sets, one soon approaches the limitations where the reliability of the final results, ionization energies and spectroscopic factors, is seriously affected.

An alternative access to the computation of the one-particle Green's function is to resort to the direct diagonalization of **B**. Here, one may make use of the well-established block Davidson procedure as described in Sec. III B for calculating a few selected roots. This one-step diagonalization is especially useful if the matrix **B** is large. On the other hand, the numerical effort grows very rapidly with the number of eigenstates being sought. Here, one meets again a situation where additional approximations or truncations become necessary in order to cope with the high-dimensional secular matrices.

In the ensuing Sec. IV A we discuss a new numerical procedure for the efficient calculation of the one-particle Green's function. The proposed procedure consists of the two major steps: a block Lanczos ''prediagonalization'' of the block $(\mathbf{K}+\mathbf{C})^{\mathrm{I}}$ and a subsequent diagonalization of the resulting smaller eigenvalue problem of the Hermitian secular matrix **B** (Dyson equation). This method makes quite naturally use of the specific structure of **B**. The evaluation of the static self-energy matrix $\mathbf{\Sigma}(\infty)$ and its numerical calculation is then discussed in Sec. IV B.

A. Block Lanczos transformation of the large (N+1)-block

To make contact with Sec. II we briefly recall the structure of the matrix **B**. It consists of three submatrices (blocks): the one-particle block $\boldsymbol{\epsilon}+\mathbf{\Sigma}(\infty)$ and the blocks $(\mathbf{K}+\mathbf{C})^{\mathrm{I}}$ and $(\mathbf{K}+\mathbf{C})^{\mathrm{II}}$ coupled to the one-particle block via the matrices of modified (effective) coupling amplitudes $\mathbf{U}^{\mathrm{I}}$ and $\mathbf{U}^{\mathrm{II}}$. The superscripts I and II refer to the spaces of physical excitations of the $(N+1)$-particle and $(N-1)$-particle systems, respectively. In the ADC(2) approximation ($2ph$-TDA) as well as the ADC(3) approximation (extended $2ph$-TDA) the spaces I and II are confined to the $2p1h$ and $2h1p$ configurations, respectively. In the case of the fourth-order scheme, ADC(4), the $3p2h$ and $3h2p$ configurations are additionally required. The one-particle block $\boldsymbol{\epsilon}+\mathbf{\Sigma}(\infty)$ corresponds to the space of $1p$ and $1h$ configurations. Without loss of generality we concentrate in the following on ADC(3). The structure of the Hermitian matrix **B** in the ADC(3) approach is shown in Fig. 1.

$1p/1h$	$2p1h$	$2h1p$
$\epsilon+\Sigma(\infty)$	$(\mathbf{U}^{\mathrm{I}})^{\dagger}$	$(\mathbf{U}^{\mathrm{II}})^{\dagger}$
$\mathbf{U}^{\mathrm{I}}$	$(\mathbf{K}+\mathbf{C})^{\mathrm{I}}$	$\mathbf{0}$
$\mathbf{U}^{\mathrm{II}}$	$\mathbf{0}$	$(\mathbf{K}+\mathbf{C})^{\mathrm{II}}$

FIG. 1. Structure of the eigenvalue problem for the Hermitian matrix **B**.

Though considerably smaller than comparable CI expansions, distinctive numerical difficulties arise from the size of the $2p1h$ and $2h1p$ configuration spaces defining the dimension of the ADC(3) matrices $(\mathbf{K}+\mathbf{C})^{\mathrm{I,II}}$. In particular, the size of the joint matrix **B** is essentially determined by that of the $2p1h$ block. As an example consider the ADC(3) calculation for the benzene molecule which is discussed below (see Sec. V). Here, the dimension is 20 746 for the $2p1h$ block and 3 254 for the $2h1p$ block in $^2A_{1g}$ symmetry (D_{2h} point group notation). Together with the one-particle block (dimension 24) the size of the matrix **B** amounts to 24 024. It is apparent that the diagonalization of **B** represents a serious obstacle in view of the large number of ionic states (typically 50–100) which are usually required in practice.

The above considerations indicate that a huge amount of computational effort can be avoided if one succeeds in truncating or approximating the very large $2p1h$ block ingenously. Here, the special structure of the secular matrix **B** comes into play. The fact that no direct coupling exists between the $2p1h$ and $2h1p$ blocks and that these blocks are energetically well separated from each other is of crucial importance. This suggests to approximate the $2p1h$ block in an appropriate manner and to investigate the influence of this approximation on the desired eigenvalues and eigenvector components associated with the ionization energies and spectral intensity coefficients, respectively, of the $(N-1)$-particle eigenstates.

Now the question arises as to how a useful approximation of the $2p1h$ block is obtained. An obvious possibility is to select out of the full $2p1h$ matrix a submatrix of fixed dimension (500 or 1000, say). The selection may be controlled, e.g., by the magnitude of coupling of the $2p1h$ and $1h$ configurations. However, in particular if the $2p1h$ block is very large, an enormous number of $2p1h$ configurations are possibly to be included in order to ensure a desired accuracy of the final results. Another and more effective way for reducing the dimension of the $2p1h$ block is to ''replace'' this block by a much smaller matrix which maintains the global information of the full $2p1h$ block. A very prac-

tical mathematical procedure which is ideally suited for this purpose is the block Lanczos algorithm. By means of this method the very large $2p1h$ block, i.e., the matrix $(\mathbf{K}+\mathbf{C})^{\mathrm{I}}$ is projected onto the subspace spanned by the Lanczos vectors generated leading to a block tridiagonal or band representation of $(\mathbf{K}+\mathbf{C})^{\mathrm{I}}$. The particular importance of the block Lanczos method as employed here is that it leads to an approximation of the $2p1h$ block, the first moments of which are exact (see Sec. III A).

The proposed method for calculating the one-particle Green's function proceeds as follows. The first step consists of supplying a set of orthonormal vectors to begin with. A particularly convenient choice of starting vectors is provided by the $N\times n$ matrix $\mathbf{U}$ built by the vectors of modified (effective) coupling amplitudes $\mathbf{U}_p$ where n, the number of columns of $\mathbf{U}$, equals the number of (occupied and unoccupied) HF orbitals and N equals the number of $2p1h$ configurations of block I. A set of orthonormal starting vectors $\mathbf{Q}^{(n)}=(q_1,q_2,\ldots,q_n)$ is then obtained by applying the modified Gram–Schmidt orthonormalization procedure to the columns of $\mathbf{U}$. This yields the $Q-R$ factorization

$$\mathbf{U}=\mathbf{Q}^{(n)}\mathbf{R}, \tag{45}$$

where $\mathbf{R}$ is an upper triangular $n\times n$ matrix. We now assume that we run the band Lanczos recursion until $j=N$, the dimension N of the matrix $\mathbf{K}+\mathbf{C}$ of block I. In this case the generated band matrix

$$\mathbf{T}^{(N)}=\mathbf{Q}^{(N)\dagger}(\mathbf{K}+\mathbf{C})\mathbf{Q}^{(N)} \tag{46}$$

simply represents an orthogonal similarity transformation of $\mathbf{K}+\mathbf{C}$. The coupling matrix $\mathbf{U}$ transforms to

$$\tilde{\mathbf{R}}=\begin{pmatrix}\mathbf{R}\\ \mathbf{0}\end{pmatrix} \tag{47}$$

which readily results from Eqs. (45) and (46). Applying the outlined block Lanczos transformation to $(\mathbf{K}+\mathbf{C})^{\mathrm{I}}$ and defining the block diagonal matrix

$$\tilde{\mathbf{Q}}=\begin{pmatrix}\mathbf{1}^{1p1h} & \mathbf{0} & \mathbf{0}\\ \mathbf{0} & \mathbf{Q} & \mathbf{0}\\ \mathbf{0} & \mathbf{0} & \mathbf{1}^{\mathrm{II}}\end{pmatrix} \tag{48}$$

one arrives at the eigenvalue problem

$$\tilde{\mathbf{B}}\tilde{\mathbf{X}}=\tilde{\mathbf{X}}\tilde{\mathbf{E}},\quad \tilde{\mathbf{X}}\tilde{\mathbf{X}}^{\dagger}=\mathbf{1}, \tag{49}$$

where

$$\tilde{\mathbf{B}}=\tilde{\mathbf{Q}}^{\dagger}\mathbf{B}\tilde{\mathbf{Q}}=\begin{pmatrix}\boldsymbol{\epsilon}+\boldsymbol{\Sigma}(\infty) & (\tilde{\mathbf{R}})^{\dagger} & (\mathbf{U}^{\mathrm{II}})^{\dagger}\\ \tilde{\mathbf{R}} & \mathbf{T} & \mathbf{0}\\ \mathbf{U}^{\mathrm{II}} & \mathbf{0} & \mathbf{K}^{\mathrm{II}}+\mathbf{C}^{\mathrm{II}}\end{pmatrix} \tag{50}$$

which is equivalent to Eqs. (18) and (19). Figure 2 provides an illustration of the structure of the Hermitian matrix $\tilde{\mathbf{B}}$.

Now observe that in $\tilde{\mathbf{B}}$, due to the particular structure of the coupling matrix $\tilde{\mathbf{R}}$, only the first n elements of the band matrix $\mathbf{T}$, i.e., the first $n\times n$ block of $\mathbf{T}$ couple directly to the one-particle block $\boldsymbol{\epsilon}+\boldsymbol{\Sigma}(\infty)$. There is no direct coupling of the ''higher'' matrix elements of $\mathbf{T}$ to the one-particle block $\boldsymbol{\epsilon}+\boldsymbol{\Sigma}(\infty)$. Furthermore, it is important to note that because of its band structure the coupling of the higher elements of the matrix $\mathbf{T}$ to the first $n\times n$ block of $\mathbf{T}$ becomes successively weaker. Remember that the moments of the ''spectra'' are conserved. This obviously allows severe truncations of the $\mathbf{T}$ matrix to dimensions j much smaller than that of the full $2p1h$ block.

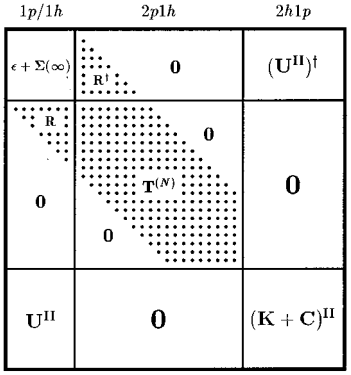

FIG. 2. Structure of the eigenvalue problem for the Hermitian matrix $\tilde{\mathbf{B}}$ after application of the block Lanczos algorithm. Because of moments conservation (see Sec. III A) one can in practical applications truncate the matrix $\mathbf{T}$ after several block Lanczos iterations.

The eigenvalues and eigenvector components of $\tilde{\mathbf{B}}$ after truncation of $\mathbf{T}$ corresponding to the energies and transition amplitudes, respectively, of the $(N-1)$-particle states represent approximations to those of the full secular problem $\mathbf{B}$. Numerical examples which demonstrate the efficiency and computational advantages of this proposed procedure are discussed in Secs. V and VI.

B. Evaluation of the static self-energy

In the following we consider the static self-energy matrix $\boldsymbol{\Sigma}(\infty)$ which appears as a part of the small $1p/1h$ block in the matrices $\mathbf{A}$ and $\mathbf{B}$, respectively. This quantity enters very sensitively the Dyson equation and an error in $\boldsymbol{\Sigma}(\infty)$ may seriously affect the reliability of the results for the single-hole main ionic states.

The basic relation for evaluating the components of $\boldsymbol{\Sigma}(\infty)$ reads[14]

$$\Sigma_{pq}(\infty)=\sum_{k,l} V_{pk[ql]}\left\{-\delta_{kl}n_k+\frac{1}{2\pi i}\oint G_{lk}(\omega)d\omega\right\}, \tag{51}$$

where the contour integration is closed in the upper complex energy plane. Here, the notation $V_{pk[ql]}=V_{pkql}-V_{pklq}$ is used for the antisymmetrized Coulomb matrix elements. Together with the Dyson equation (9) and Eq. (11) the above relation establishes an iterative procedure for the consistent calculation of both the static self-energy $\boldsymbol{\Sigma}(\infty)$ and the one-particle Green's function $\mathbf{G}(\omega)$, once the dynamic self-energy $\mathbf{M}(\omega)$ or an approximation of it is given.

In practice, however, the self-consistent procedure is expensive since the residues of *all* $(N-1)$-particle eigenstates

are to be determined from the secular matrices **A** or **B**. Replacing $\mathbf{G}(\omega)$ in Eq. (51) by the first two terms of the Dyson expansion

$$\mathbf{G}(\omega)=\mathbf{G}^0(\omega)+\mathbf{G}^0(\omega)\mathbf{\Sigma}(\omega)\mathbf{G}^0(\omega)+\cdots \tag{52}$$

and considering Eq. (11) one arrives at

$$\Sigma_{pq}(\infty)=\sum_{k,l}\ V_{pk[ql]}\ \frac{1}{2\pi i}\ \oint d\omega\ G^0_{ll}(\omega)[\Sigma_{lk}(\infty)+M_{lk}(\omega)]G^0_{kk}(\omega), \tag{53}$$

which in general represents an excellent approximation to the fully iterated result of Eq. (51). After performing part of the contour integrations the problem of determining $\mathbf{\Sigma}(\infty)$ reduces to the single matrix inversion

$$\Sigma_{pq}(\infty)-\sum_{k,l}\ V_{pk[ql]}\left[\frac{\overline{n_l}n_k}{\epsilon_k-\epsilon_l}+\frac{n_l\overline{n_k}}{\epsilon_l-\epsilon_k}\right]\Sigma_{lk}(\infty)=b_{pq} \tag{54}$$

entirely defined in the space of the one-particle and one-hole configurations. The inhomogeneities b_{pq} are given by

$$b_{pq}=\sum_{k,l}\ V_{pk[ql]}\ \frac{1}{2\pi i}\ \oint d\omega\ G^0_{ll}(\omega)M_{lk}(\omega)G^0_{kk}(\omega), \tag{55}$$

where the contour integral closes in the upper half of the complex energy plane. The error introduced by the truncation of the Dyson expansion (52) is of fifth order perturbation theory, i.e., $\mathbf{\Sigma}(\infty)$ is complete through fourth order if the third-order approximation, ADC(3), for the dynamic self-energy $\mathbf{M}(\omega)$ is employed. The major numerical obstacle is concealed in the inhomogeneities b_{pq} requiring the contour integrations

$$Q_{kl}=\frac{1}{2\pi i}\ \oint d\omega\ G^0_{ll}(\omega)M_{lk}(\omega)G^0_{kk}(\omega). \tag{56}$$

For an explicit spectral representation of $\mathbf{M}(\omega)$, see Eqs. (12) and (13), the result is

$$Q_{kl}=Q^{\mathrm{I}}_{kl}+Q^{\mathrm{II}}_{kl}, \tag{57}$$

$$Q^{\mathrm{I}}_{kl}=\sum_{\mu\in\{N+1\}} m^{(\mu)}_l m^{(\mu)*}_k\left[\frac{-n_l n_k}{(\epsilon_k-\omega_\mu)(\epsilon_l-\omega_\mu)}+\frac{n_k\overline{n_l}}{(\epsilon_k-\epsilon_l)(\epsilon_k-\omega_\mu)}-\frac{n_l\overline{n_k}}{(\epsilon_k-\epsilon_l)(\epsilon_l-\omega_\mu)}\right], \tag{58}$$

$$Q^{\mathrm{II}}_{kl}=\sum_{\mu\in(N-1)} m^{(\mu)}_l m^{(\mu)*}_k\left[\frac{\overline{n_l}n_k}{(\epsilon_k-\omega_\mu)(\epsilon_l-\omega_\mu)}-\frac{n_l\overline{n_k}}{(\epsilon_k-\epsilon_l)(\epsilon_k-\omega_\mu)}+\frac{\overline{n_l}n_k}{(\epsilon_k-\epsilon_l)(\epsilon_l-\omega_\mu)}\right]. \tag{59}$$

The evaluation of these quantities requires, in principle, the separate *full* diagonalization of the secular matrices $\mathbf{K}+\mathbf{C}$ of the blocks I and II. This poses considerable numerical difficulties due to the large dimension of these matrices. Numerical strategies which avoid or circumvent the full diagonalization of $\mathbf{K}+\mathbf{C}$ have been discussed in Ref. 43. There, two alternative methods, namely an inversion method (Jacobi iteration[44]) and a single-vector Lanczos diagonalization method, have been considered for the efficient calculation of the integrals Q_{kl}. Here, we complement these investigations by introducing a block or band Lanczos diagonalization procedure which also allows for a direct and efficient access to the integrals Q_{kl}.

As with the single-vector Lanczos method for diagonalizing $\mathbf{K}+\mathbf{C}$ described in Ref. 43, the block Lanczos method operates by generating an increasing basis of Lanczos vectors and computing the projection of $\mathbf{K}+\mathbf{C}$ onto this basis. Upon performing the algorithm (34) outlined in Sec. III A one arrives after j band (i.e., $J=[j/n]$ block) iterations at the band (block tridiagonal) matrix $\mathbf{T}^{(j)}$ of Eq. (33). The diagonalization of $\mathbf{T}^{(j)}$ yields a set of j eigenvalues $\tilde{\omega}_\mu$ representing approximations to the exact eigenvalues of $\mathbf{K}+\mathbf{C}$.

The Dyson amplitude $m^{(\mu)}_p$ is the overlap of the modified coupling amplitude $\mathbf{U}_p$—i.e., the pth column vector of the coupling matrix **U**—with the μth eigenvector of $\mathbf{K}+\mathbf{C}$. As starting vectors one hence has to choose the (Gram–Schmidt orthonormalized) coupling amplitudes. Thus starting the process with the matrix $\mathbf{U}^{\mathrm{I}}$ of column vectors $\mathbf{U}^{\mathrm{I}}_p$, where the number of columns equals the number of occupied *and* unoccupied orbitals, one may compute all the matrix elements Q^{I}_{kl} via a simple block Lanczos diagonalization of $\mathbf{K}+\mathbf{C}$ associated with the larger block I. Similarly, employing the starting matrix $\mathbf{U}^{\mathrm{II}}$ one obtains all matrix elements Q^{II}_{kl} by diagonalizing the secular matrix $\mathbf{K}+\mathbf{C}$ of the smaller block II. In practical applications convergence of the elements $Q^{\mathrm{I,II}}_{kl}$ to 10^{-9} is usually achieved within 12 to 15 block iterations.

The procedure just described has the practical advantage that the pseudospectra obtained for the larger block I can be reused to build the secular matrix $\tilde{\mathbf{B}}$ of Eq. (50). A closer inspection of Eqs. (58) and (59) reveals that it suffices to run the algorithm with a smaller block size of $\mathbf{U}^{\mathrm{I}}$ and $\mathbf{U}^{\mathrm{II}}$ comprising the occupied *or* unoccupied orbitals only. This clearly restricts the amount of multiplications of the matrix $\mathbf{K}+\mathbf{C}$ and the vectors $\mathbf{U}_p$. Proceeding in this way one has to evaluate and store the overlaps $\mathbf{U}^\dagger_p q_i$, $i=1,2,\ldots,j$, for each occupied or unoccupied orbital p. After j band Lanczos iterations are performed, diagonalize $\mathbf{T}^{(j)}$ and compute its *full* eigenvector matrix $\mathbf{X}^{(j)}$. The matrix of approximate Dyson amplitudes $\tilde{m}^{(\mu)}_p$ is given by

$$\tilde{\mathbf{m}}=\mathbf{U}^\dagger\mathbf{Q}^{(j)}\mathbf{X}^{(j)}=\tilde{\mathbf{R}}^\dagger\mathbf{X}^{(j)}. \tag{60}$$

In substituting the exact spectral energies ω_μ and Dyson amplitudes $m^{(\mu)}_p$ in Eqs. (58) and (59) by those of the block Lanczos pseudospectrum one obtains an approximation for the matrix elements Q_{kl}. The second part of Eq. (60) shows that only the first n components of the eigenvectors are needed [cf. Eq. (47)], where n denotes the dimension of the $1p/1h$ block. This property significantly reduces the numerical effort.[10]

It should be mentioned that the block Lanczos diagonalization procedure becomes expensive when a large number of band iterations j is required. In contrast to the inversion

method,[43] however, both the single-vector and block Lanczos methods guarantee the convergence of the integrals Q_{kl}.

V. AN ILLUSTRATIVE EXAMPLE: THE IONIZATION SPECTRUM OF BENZENE

To illustrate the performance of the block Lanczos transformation described above in realistic applications we have calculated the vertical-electronic ionization energies and spectral intensities (pole strengths) of the valence ionic states in benzene using the ADC(3) approximation for the one-particle Green's function. The approximate values of these quantities obtained via the diagonalization of the block Lanczos ''prediagonalized'' secular matrix $\tilde{\mathbf{B}}$ are compared to the corresponding ''exact'' values resulting from the one-step ''direct'' diagonalization of the full secular problem **B**. The computations have been performed on an IBM 3090 computer.

The required input data for the Green's function calculations,[45] molecular orbital energies and Coulomb integrals, were generated from *ab initio* Hartree–Fock self-consistent field (HF-SCF) calculations at the neutral-molecule ground state geometry employing the experimental equilibrium distances $R_{C-C}=1.397$ Å and $R_{C-H}=1.084$ Å.[46] A contracted double-zeta plus polarization (DZP) basis set was used consisting of $4s,2p,1d$ Cartesian Gaussians on each carbon and $2s,1p$ on each hydrogen.[47,48] The exponents for the d-type polarization functions on carbon and for the p-type polarization functions on hydrogen are 0.6 and 0.75, respectively. The ground state HF total energy thus resulting is $-230.728\,603$ a.u. The total number of molecular orbitals is 126.

In the Green's function calculations the orbital space has almost completely been exhausted. Only the $C1s$ core occupied orbitals and their unoccupied (virtual) counterparts have been left out of consideration. This leaves a total of 114 (15 occupied and 99 virtual) valence orbitals to be included when constructing the configuration spaces of the blocks I and II. To introduce from the outset an *a priori* reduction of the size of the secular problem both the spin and spatial symmetries have been exploited. The spin-free expressions for the elements of the ADC(3) matrices $\mathbf{K}+\mathbf{C}$ and **U** employed here are given in Ref. 21. The spatial symmetry has been exploited to the extent of the largest one-dimensional (Abelian) subgroup of the full symmetry group, i.e., D_{2h} in the case of benzene. The construction of symmetry-adapted configurations is then trivial. Thus for each irreducible representation there results a decoupled eigenvalue problem for the matrix **B**. The dimensions of the subblocks of **B** and of **B** itself as arising within the D_{2h} point group are listed in Table I. Here, we shall confine ourselves to the $^2A_{1g}$ symmetry only. For this symmetry the dimension was 20 746 for $(\mathbf{K}+\mathbf{C})^{\mathrm{I}}$ and 3 254 for $(\mathbf{K}+\mathbf{C})^{\mathrm{II}}$. These matrices are sparse with 6.6% and 22.3% nonzero elements, respectively. Together with the one-particle block $1p/1h$ whose dimension is 24 (equal to the number of occupied and unoccupied orbitals of a_{1g} symmetry) the size of the joint matrix **B** amounts to 24 024. We note that the solutions of the eigenvalue problem for **B** of $^2A_{1g}$ symmetry in D_{2h} are readily reclassified with respect to the full symmetry point group of benzene, D_{6h}, yielding the eigenstates of $^2E_{2g}$ and $^2A_{1g}$ symmetry.

TABLE I. Dimensions of the ADC(3) secular problems **B** for benzene as arising for the different symmetry species within the D_{2h} point group.

Symmetry	p	h	$2p1h$	$2h1p$	Joint dimension
$^2A_{1g}$	20	4	20 746	3254	24 024
$^2A_{1u}$	6	0	16 014	2316	18 336
$^2B_{1g}$	16	2	20 564	3226	23 808
$^2B_{1u}$	8	1	16 183	2342	18 534
$^2B_{2g}$	5	1	16 021	2309	18 336
$^2B_{2u}$	21	3	20 739	3261	24 024
$^2B_{3g}$	8	1	16 177	2348	18 534
$^2B_{3u}$	15	3	20 571	3219	23 808

The static self-energy matrix $\mathbf{\Sigma}(\infty)$ appearing in the one-particle block was determined via the free one-particle Green's function (direct) approach as described in Sec. IV B (see also Refs. 41 and 43). The ADC(3) expressions for $\mathbf{K}+\mathbf{C}$ and **U** were employed. This allows for an approximation of $\mathbf{\Sigma}(\infty)$ that is complete through fourth-order perturbation theory and that includes partial contributions of certain perturbation terms in all higher orders. The block Lanczos algorithm was used to calculate the integrals Q_{kl} of Eqs. (57)–(59). On average about *15* block iterations per symmetry were required to achieve convergence of the elements Q_{kl} to 10^{-9}. Within this convergence threshold an accuracy of about 10^{-6} eV for the matrix elements $\Sigma_{kl}(\infty)$ is obtained.

Next we have generated the elements of the band matrix **T** of the $2p1h$ block using the block Lanczos algorithm. Starting with matrix $\mathbf{U}^{\mathrm{I}}$ of column vectors $\mathbf{U}^{\mathrm{I}}_p$ where the number of columns equals the number of HF orbitals in a_{1g} symmetry, *five* block iterations were performed leading to a **T** matrix of dimension 120. This defines our pseudospectrum 1. To study convergence further five block iterations were appended to the previous run thus yielding a total of *ten* block iterations. In this case the dimension of the resulting **T** matrix is 240 (pseudospectrum 2). Note that the dimensions of these projection matrices are substantially smaller than that of the full secular matrix $(\mathbf{K}+\mathbf{C})^{\mathrm{I}}$ (dimension 20 746). In the realization of the calculations both the coupling matrix **R** and the **T** matrices were kept in fast memory. This was no longer possible for the matrix $(\mathbf{K}+\mathbf{C})^{\mathrm{I}}$ which was therefore held on disk.

Once the block Lanczos pseudospectrum of the $2p1h$ block has been computed the matrix $\tilde{\mathbf{B}}$ was then diagonalized using the block Davidson procedure. The calculations were performed as described in Sec. III B. The results obtained on the valence ionic states of $^2E_{2g}$ and $^2A_{1g}$ symmetry are collected in Tables II and III (here and in the following the symmetry labels of the full spatial point group of benzene, D_{6h}, are used). In the tables the notations $I_n^{(J)}$ and $P_{pn}^{(J)}$ are employed for the ionization energies and pole strengths after the Jth block Lanczos iteration, respectively. For comparison the corresponding ''exact'' values, I_n and P_{pn}, of the direct diagonalization of the full problem **B** are also shown. We mention that a detailed discussion of the present results on

TABLE II. Approximate ionization energies $I_n^{(J)}$ up to 30 eV with major pole strengths $[P_{pn}^{(J)} \geqslant 0.01]$ of the valence ionic states with $^2E_{2g}$ symmetry of benzene obtained via the diagonalization of the prediagonalized secular matrix $\tilde{\mathbf{B}}$. The superscript J denotes the number of block Lanczos iterations performed in calculating the pseudospectrum of the $2p1h$ block. The corresponding ''exact'' values of the direct diagonalization of the full secular problem **B** are denoted as I_n and P_{pn}. Also shown are the absolute errors in the ionization energies, $|I_n - I_n^{(J)}|$, as well as in the pole strengths, $|P_{pn} - P_{pn}^{(J)}|$. The numbers in parentheses are the powers of ten with which the entries are to be multiplied. All energies in eV.

Orbital p	$I_n^{(5)}$	$\lvert I_n - I_n^{(5)}\rvert$	$P_{pn}^{(5)}$	$\lvert P_{pn} - P_{pn}^{(5)}\rvert$	$I_n^{(10)}$	$\lvert I_n - I_n^{(10)}\rvert$	$P_{pn}^{(10)}$	$\lvert P_{pn} - P_{pn}^{(10)}\rvert$	I_n	P_{pn}
$3e_{2g}$	12.226 974	6.60(−4)	0.896 694	8.70(−5)	12.227 632	2.00(−6)	0.896 613	6.00(−6)	12.227 634	0.896 607
$2e_{2g}$	18.980 895	6.00(−6)	0.017 309	2.10(−5)	18.980 901	<1.00(−6)	0.017 288	<1.00(−6)	18.980 901	0.017 288
	19.106 338	3.80(−5)	0.105 199	7.40(−5)	19.106 376	<1.00(−6)	0.105 127	2.00(−6)	19.106 376	0.105 125
	19.536 669	1.06(−4)	0.305 460	8.90(−5)	19.536 775	<1.00(−6)	0.305 372	1.00(−6)	19 536 775	0.305 371
	19.909 481	6.80(−5)	0.200 367	1.01(−4)	19.909 549	<1.00(−6)	0.200 471	3.00(−6)	19.909 549	0.200 468
	20.583 741	9.00(−6)	0.029 338	9.00(−6)	20.583 750	<1.00(−6)	0.029 347	<1.00(−6)	20.583 750	0.029 347
	20.857 246	6.00(−6)	0.017 761	3.00(−6)	20.857 252	<1.00(−6)	0.017 764	<1.00(−6)	20.857 252	0.017 764
	21.217 717	2.30(−5)	0.079 763	1.90(−5)	21.217 740	<1.00(−6)	0.079 783	1.00(−6)	21.217 740	0.079 782
	21.883 285	1.10(−5)	0.039 131	9.00(−6)	21.883 296	<1.00(−6)	0.039 140	<1.00(−6)	21.883 296	0.039 140
	25.687 004	3.00(−6)	0.017 801	1.00(−6)	25.687 007	<1.00(−6)	0.017 802	<1.00(−6)	25.687 007	0.017 802
	27.786 274	3.00(−6)	0.013 791	1.00(−6)	27.786 277	<1.00(−6)	0.013 791	1.00(−6)	27.786 277	0.013 790

the satellite states has been published recently.[49] There, the results of a more extensive ADC(3) calculation based on a triple-zeta-valence plus polarization (TZVP) basis set built up of $5s,3p,1d$ Cartesian Gaussians on each carbon and $3s,1p$ on each hydrogen[47,50] are also included. The exponents chosen for the polarization functions in the TZVP basis set are the same as those used in the DZP basis set.

Let us now discuss the outcome of the calculations. Using pseudospectrum 1, quite a good agreement with the results of the direct diagonalization of the full problem **B** is already obtained. It is generally recognized that the absolute error in the ionization energies, i.e., the difference $|I_n - I_n^{(5)}|$ decreases upon going from the outer-valence energy regime to the inner-valence energy regime of the ionization spectrum. This is easily understood since, due to the larger energy gap, the approximated $2p1h$ block has much less influence on the inner-valence ionic levels than on the outer-valence ionic levels which are comparatively close to the $2p1h$ block. More specifically, for the lowest $^2E_{2g}$ state the discrepancy between the computed approximate ionization energy $I_n^{(5)}$ and the corresponding ''exact'' value I_n, where **B** was diagonalized by the block Davidson procedure alone, is 6.60×10^{-4} eV. The absolute error in the corresponding pole strength, $|P_{pn} - P_{pn}^{(5)}|$, is also small (8.70×10^{-5}). For the deeper-lying valence ionic states of $^2E_{2g}$ symmetry the calculations yield a maximum error of 1.06×10^{-4} eV for the ionization energy and of 1.01×10^{-4} for the pole strength. A similar trend is observed for the valence ionic states of $^2A_{1g}$ symmetry. As can be seen from Table III, the ionization energy and pole strength of the $^2A_{1g}$ state lowest in energy are reproduced to within 3.38×10^{-4} eV and 5.50×10^{-5}, respectively, of the corresponding ''exact'' values. The largest

TABLE III. Approximate ionization energies $I_n^{(J)}$ up to 30 eV with major pole strengths $[P_{pn}^{(J)} \geqslant 0.01]$ of the valence ionic states with $^2A_{1g}$ symmetry of benzene obtained via the diagonalization of the prediagonalized secular matrix $\tilde{\mathbf{B}}$. The superscript J denotes the number of block Lanczos iterations performed in calculating the pseudospectrum of the $2p1h$ block. The corresponding ''exact'' values of the direct diagonalization of the full secular problem **B** are denoted as I_n and P_{pn}. Also shown are the absolute errors in the ionization energies, $|I_n - I_n^{(J)}|$, as well as in the pole strengths, $|P_{pn} - P_{pn}^{(J)}|$. The numbers in parentheses are the powers of ten with which the entries are to be multiplied. All energies in eV.

Orbital p	$I_n^{(5)}$	$\lvert I_n - I_n^{(5)}\rvert$	$P_{pn}^{(5)}$	$\lvert P_{pn} - P_{pn}^{(5)}\rvert$	$I_n^{(10)}$	$\lvert I_n - I_n^{(10)}\rvert$	$P_{pn}^{(10)}$	$\lvert P_{pn} - P_{pn}^{(10)}\rvert$	I_n	P_{pn}
$3a_{1g}$	17.353 573	3.38(−4)	0.797 029	5.50(−5)	17.353 910	1.00(−6)	0.796 977	3.00(−6)	17.353 911	0.796 974
	19.959 252	7.00(−6)	0.019 585	4.00(−6)	19.959 259	<1.00(−6)	0.019 589	<1.00(−6)	19.959 259	0.019 589
	21.814 986	1.10(−5)	0.043 152	3.00(−6)	21.814 997	<1.00(−6)	0.043 155	<1.00(−6)	21.814 997	0.043 155
	25.794 423	3.00(−6)	0.018 421	<1.00(−6)	25.794 426	<1.00(−6)	0.018 421	<1.00(−6)	25.794 426	0.018 421
$2a_{1g}$	25.886 852	4.00(−6)	0.029 751	5.00(−6)	25.886 856	<1.00(−6)	0.029 745	1.00(−6)	25.886 856	0.029 746
	26.134 281	2.00(−6)	0.009 600	2.00(−6)	26.134 283	<1.00(−6)	0.009 597	1.00(−6)	26.134 283	0.009 598
	26.781 181	1.30(−5)	0.095 064	1.01(−4)	26.781 194	<1.00(−6)	0.094 965	2.00(−6)	26.781 194	0.094 963
	26.849 326	2.60(−5)	0.189 995	2.00(−6)	26.849 352	<1.00(−6)	0.189 987	6.00(−6)	26.849 352	0.189 993
	26.992 161	2.40(−5)	0.177 282	7.40(−5)	26.992 185	<1.00(−6)	0.177 356	<1.00(−6)	26.992 185	0.177 356
	27.378 993	1.40(−5)	0.094 335	2.10(−5)	27.379 007	<1.00(−6)	0.094 358	2.00(−6)	27.379 007	0.094 356
	28.836 113	1.00(−6)	0.014 475	1.00(−6)	28.836 114	<1.00(−6)	0.014 473	3.00(−6)	28.836 114	0.014 476
	29.048 785		0.064 144		29.048 792		0.064 151		a	
	29.349 252		0.010 598		29.349 253		0.010 599		a	
	29.649 414		0.013 971		29.649 416		0.013 971		a	

[a]The diagonalization procedure for these high-energy roots of **B** did not converge.

deviations in the energies and pole strengths found for the other ionic states of $^2A_{1g}$ symmetry are 2.60×10^{-5} eV and 1.01×10^{-4}, respectively. We mention that similar results have been obtained for the other symmetry species not discussed here.

Using pseudospectrum 2, a considerable improvement over the previous results is obtained. As is made available by Tables II and III, both the ionization energies and pole strengths of all the valence ionic states of $^2E_{2g}$ and $^2A_{1g}$ symmetry are more or less reproduced to within about 6 ''exact'' digits. As a remarkable outcome of our investigations we would like to emphasize that we did not achieve convergence for the three states of $^2A_{1g}$ symmetry highest in energy when directly diagonalizing the full secular problem **B**. This further underlines the excellent performance of the block Lanczos method as employed here; the secular matrices $\tilde{\mathbf{B}}$ to be finally diagonalized are smaller and hence the diagonalization process is numerically more stable than for the matrices **B**.

The above discussion of efficiency essentially compares the error in the final results, i.e., in the ionization energies and pole strengths. A further relevant aspect concerns the gain in computation time by the two-step diagonalization procedure with respect to the direct diagonalization of full secular problem. The time-determining step in the block Lanczos algorithm is the multiplication of the matrices $\mathbf{K}+\mathbf{C}$ and **U**. The other operations have negligible cost and will not be considered here. The characteristic CPU time for *one* block iteration was 250 s on an IBM 3090 computer. Thus about 1250 and 2500 s were used up in generating the pseudospectra 1 and 2, respectively, considered here. The subsequent diagonalization of the matrix $\tilde{\mathbf{B}}$ took about 900 s. For comparison, the diagonalization time of the full problem **B** was approximately 8000 s. Hence, we find that the two-step procedure is between *four* and *two* times faster than the direct diagonalization of **B**. It should be mentioned that these efficiency factors substantially increase with the size of the molecule, the orbital basis set employed, and the number of roots to be computed. Moreover, one may expect that a more efficient (vectorized) computer code for the block Lanczos algorithm will further increase the performance of the proposed procedure.

VI. COMPLETE VALENCE-SHELL IONIZATION SPECTRA OF BeF_4^{2-}, BeF_3^-, AND BeF_2

The diagonalization of the full secular matrix **B** (Dyson equation) whose eigenvalues and eigenvectors determine the one-particle Green's function is generally expensive. The proposed procedure introduced in Sec. IV uses the block Lanczos algorithm as a natural and convenient tool for reducing the dimension of the secular problem, leading to an enhanced numerical stability of the diagonalization process. This reduction of the size of the secular problem is particularly important in applications where the treatment of the full problem **B** becomes computationally extremely cumbersome. In cases where a large number of very closely lying states in the inner-valence ionization region are present, the diagonalization of **B** (via block Davidson) cannot be carried out in this part of the spectrum. In this section we describe an application for such a case.

In recent articles (see Refs. 51 and 52) the existence and properties of the *free* doubly negative molecular systems MF_4^{2-} (M=Be, Mg, and Ca) have been discussed. These dianions were found to be stable with respect to both fragmentation into MF_3^- and F^- and to electron loss. The stability to electron loss has been established by computing the vertical-electronic ionization energies of the outer-valence (main) anionic states of the MF_4^{2-} dianions using the one-particle Green's function approach. In the following we give an account of the computational details of the calculations that we have performed on the complete valence-shell ionization regime of the above dianions. In addition, we also report on the calculated ionization spectra of the corresponding anions and neutral systems. As representative examples of these systems we discuss the results obtained for BeF_4^{2-}, BeF_3^-, and BeF_2. The computed spectra of the homologous systems MF_4^{2-}, MF_3^-, and MF_2 (M=Mg and Ca) are similar to those of the beryllium fluorides. They are discussed in Ref. 53.

The valence-shell ionization spectra of BeF_4^{2-}, BeF_3^-, and BeF_2 have been calculated using the ADC(3) approximation for the one-particle Green's function. The orbital energies and Coulomb integrals required for the Green's function calculations were obtained from ground state HF-SCF calculations using the respective optimized CI geometries of the above systems. Details on the geometry optimization calculations and the basis sets employed are given in Refs. 51 and 52. As for benzene, the spatial symmetry has been exploited to the extent of the respective largest one-dimensional subgroups of the full point group, i.e., D_2, C_{2v}, and D_{2h} in the case of BeF_4^{2-}, BeF_3^-, and BeF_2, respectively. The orbital space has essentially been exhausted. With the exception of the $F1s$ core occupied orbitals and their unoccupied counterparts all the remaining orbitals have been maintained. For the largest system considered here, BeF_4^{2-}, the resulting configuration spaces of the blocks I and II with largest dimensions are 23 913 and 5 421, respectively ($^2A_1$ in D_2 point group symmetry). The various computational steps of the ADC(3) calculations proceeded as described in the preceding section for benzene. For each beryllium fluoride system, the total number of block iterations performed in generating the respective pseudospectra was *ten*. In the case of BeF_4^{2-}, the largest eigenvalue problem for the prediagonalized secular matrix $\tilde{\mathbf{B}}$ was of dimension 5707 ($^2A_1$, D_2 notation). By contrast, the corresponding full secular problem **B** is of dimension 29 360.

The results, ionization energies and spectral intensities (pole strengths), obtained for BeF_4^{2-}, BeF_3^-, and BeF_2 are collected in Table IV. In addition, the calculated ionization spectra are displayed in Fig. 3 in the shape of a line spectrum. The position and height of each line are given by the computed ionization energy and pole strength, respectively. The number above each line indicates the orbital out of which ionization takes place.

Before discussing the results let us first describe the most critical problems arising in the calculations of the ion-

TABLE IV. Vertical-electronic ionization energies I_n and spectral intensity coefficients P_{pn} of BeF_4^{2-}, BeF_3^-, and BeF_2 calculated using the ADC(3) Green's function approach. Ten block Lanczos iterations have been performed on $(\mathbf{K}+\mathbf{C})^l$ and subsequently the resulting matrix $\tilde{\mathbf{B}}$ has been diagonalized using the block Davidson procedure. The states with $P_{pn} \geqslant 0.01$ are shown. All energies in eV.

BeF_4^{2-}				BeF_3^-				BeF_2			
Orbital	Hartree–Fock	Green's function		Orbital	Hartree–Fock	Green's function		Orbital	Hartree–Fock	Green's function	
p	$-\epsilon_p$	I_n	P_{pn}	p	$-\epsilon_p$	I_n	P_{pn}	p	$-\epsilon_p$	I_n	P_{pn}
$1t_1$	3.47	1.88	0.92	$1a_2'$	9.47	7.86	0.92	$1\pi_g$	17.26	15.85	0.93
$4t_2$	3.89	2.38	0.92	$1e''$	9.97	8.46	0.92	$1\pi_u$	17.86	16.57	0.93
$1e$	4.47	2.93	0.92	$4e'$	10.14	8.61	0.92	$4\sigma_g$	18.89	17.62	0.93
$3t_2$	5.53	4.10	0.92	$1a_2''$	10.90	9.52	0.92	$3\sigma_u$	19.27	17.89	0.92
$4a_1$	6.40	5.01	0.92	$3e'$	11.81	10.35	0.92				
				$4a_1'$	12.22	10.81	0.92				
$2t_2$	28.69	24.78	0.04	$2e'$	35.01	30.80	0.01	$3\sigma_g$	42.51	38.90	0.81
		24.84	0.02			31.08	0.01			41.95	0.06
		24.92	0.04			31.23	0.16			45.15	0.02
		24.96	0.06			31.33	0.32	$2\sigma_u$	42.73	39.09	0.79
		24.99	0.22			31.39	0.05			41.95	0.07
		25.11	0.23			31.45	0.16			45.16	0.02
		25.22	0.02			31.52	0.03				
		25.31	0.06			31.54	0.01				
		25.40	0.06			31.68	0.02				
$3a_1$	29.20	25.46	0.05			35.45	0.01				
		25.52	0.20			38.00	0.01				
		25.58	0.31	$3a_1'$	35.33	31.19	0.01				
		25.67	0.14			31.54	0.01				
		25.84	0.07			31.55	0.04				
		26.03	0.01			31.66	0.03				
		28.38	0.02			31.73	0.72				
						35.45	0.02				
						38.04	0.01				

ization spectra of the systems BeF_4^{2-} and BeF_3^-. Whereas the block Davidson algorithm could be straightforwardly applied to the matrix $\tilde{\mathbf{B}}$ to extract the desired information on the outer-valence part of the spectrum, serious computational difficulties emerged in calculating inner-valence ionic states. The convergence problems of the block Davidson method encountered in the inner-valence ionization region are due to the large number of closely lying states in that part of the spectrum. To overcome these problems a modification of the initial subspace selection for the block Davidson iterations was adopted. In the usual procedure the starting subspace vectors are simply selected as an $N \times n$ ''unit'' matrix $\mathbf{Q}^{(n)}$ with elements $Q_{im} = \delta_{im}$, where n is equal to the number of occupied orbitals and N denotes the dimension of the prediagonalized matrix $\tilde{\mathbf{B}}$. In the problematic cases we augmented this starting basis set by additional unit vectors selected using a second-order perturbation theory criterion as follows. The full list of $2h1p$ and $2p1h$ configurations is ordered according to their summed second-order contribution to the $1h$ inner-valence states and a suitable number of the largest contributing ones is then added to the starting basis. Out of the thus obtained basis vectors a maximum number of 600 basis vectors has been considered. In the block Davidson diagonalization of $\tilde{\mathbf{B}}$ the large number of about 70 block iteration cycles were required to achieve convergence for all inner-valence ionic states, leading to $\mathbf{S}$ matrices with dimensions around 1100. Without the reduction of dimension when going from $\mathbf{B}$ to $\tilde{\mathbf{B}}$, the diagonalization of all inner-valence states is hardly possible.

We now turn to the discussion of the computed ionization spectra of BeF_4^{2-}, BeF_3^-, and BeF_2. In its ground state the BeF_4^{2-} dianion is well described by the T_d electronic configuration $(core)^{10}(3a_1)^2(2t_2)^6(4a_1)^2(3t_2)^6(1e)^4(4t_2)^6 \times (1t_1)^6$. As can be seen in Fig. 3 the spectrum of BeF_4^{2-} consists of two groups of closely spaced lines which are separated by a large energy gap ($\sim$20 eV). The first group of lines at lowest ionization energy results from the removal of electrons out of the outer-valence orbitals $1t_1$, $4t_2$, $1e$, $3t_2$, and $4a_1$. These orbitals essentially derive from the $2p$ levels of fluorine (F$2p$ lone pairs), the highest occupied of which, $1t_1$, is nonbonding with respect to the central beryllium atom. The second group of lines at higher binding energy arises from the ionization out of the inner-valence orbitals $2t_2$ and $3a_1$ which are mainly of fluorine $2s$ character. These lines are satellite lines and correspond to $2h1p$ configurations involving electron excitations from the outer-valence occupied to low-lying unoccupied (virtual) orbitals accompanying the ionization of an electron out of an outer-valence orbital. They acquire their intensity by borrowing it from the $2s$ main states. According to the classification scheme presented in Ref. 15 these satellites are final-state or correlation satellites. The present calculation yields a total of nine satellite lines of $^2T_2$ symmetry and a total of seven satellite lines of $^2A_1$ symmetry with pole strengths greater or equal to

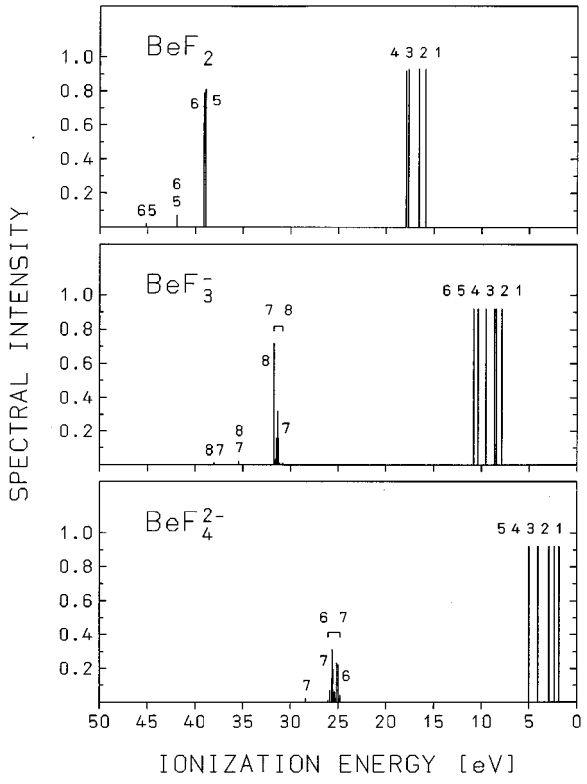

FIG. 3. Valence-shell ionization spectra of BeF_2, BeF_3^-, and BeF_4^{2-} calculated using the ADC(3) Green's function approach. The states with pole strengths greater or equal to 0.01 are shown. The number above each line specifies the orbital out of which ionization takes place. The assignment is as follows: $1=1\pi_g$, $2=1\pi_u$, $3=4\sigma_g$, $4=3\sigma_u$, $5=3\sigma_g$, and $6=2\sigma_u$ (BeF_2); $1=1a_2'$, $2=1e''$, $3=4e'$, $4=1a_2''$, $5=3e'$, $6=4a_1'$, $7=2e'$, and $8=3a_1'$ (BeF_3^-); $1=1t_1$, $2=4t_2$, $3=1e$, $4=3t_2$, $5=4a_1$, $6=2t_2$, and $7=3a_1$ (BeF_4^{2-}).

0.01. The most intense $^2T_2$ satellites are predicted to appear at 24.99 and 25.11 eV and to possess pole strengths of 0.22 and 0.23, respectively. The most intense $^2A_1$ satellites are predicted to lie at 25.52 and 25.58 eV and to have pole strengths of 0.20 and 0.31, respectively. As one can see from the figure, $2t_2$ and $3a_1$ main states cannot be identified, their intensity has spread over many lines. One encounters the phenomenon of the breakdown of the orbital picture of ionization.[15]

The ionization spectrum of BeF_3^- shown in Fig. 3 is similar to that of BeF_4^{2-} discussed above. In the outer-valence energy regime the spectrum exhibits six main ionization lines all possessing a pole strength of 0.92. In the order of increasing ionization energy these lines are associated with the ejection of electrons out of the orbitals $1a_2'$, $1e''$, $4e'$, $1a_2''$, $3e'$, and $4a_1'$ in accordance with the D_{3h} ground state electronic configuration $(core)^8(3a_1')^2(2e')^4 \times (4a_1')^2(3e')^4(1a_2'')^2(4e')^4(1e'')^4(1a_2')^2$ of the BeF_3^- anion. As for the outer-valence orbitals of BeF_4^{2-}, these orbitals are essentially built up of fluorine $2p$ components, the highest occupied orbital, $1a_2'$, is nonbonding with respect to beryllium. The rich satellite structure at about 31 eV binding energy originates from the ionization out of the inner-valence orbitals $3a_1'$ and $2e'$ which have mainly fluorine $2s$ character. Further weak satellite lines of $^2A_1'$ and $^2E'$ symmetry are predicted to appear at somewhat higher energy. As for the BeF_4^{2-} dianion these satellite lines arise due to correlation effects in the final states and thus can be classified as correlation satellites. The major portion of the pole strength (0.72) available for the $3a_1'$ orbital is confined in the ''main'' state at 31.73 eV; the most intense lines emerging from the ionization of the $2e'$ orbital are the ones at 31.23, 31.33, and 31.45 eV having pole strengths of 0.16, 0.32, and 0.16, respectively.

Finally, we briefly discuss the results for BeF_2. The calculated ionization spectrum in Fig. 3 of this molecule which possesses the $D_{\infty h}$ ground state electronic configuration $(core)^6(2\sigma_u)^2(3\sigma_g)^2(3\sigma_u)^2(4\sigma_g)^2(1\pi_u)^4(1\pi_g)^4$ is rather simple. It consists of four outer-valence main ionization lines originating from the removal of electrons out of the orbitals $1\pi_g$, $1\pi_u$, $4\sigma_g$, and $3\sigma_u$. The ionization of the inner-valence orbital $3\sigma_g$ is predicted by the present calculation to result in a ''main'' line at 38.90 eV with a pole strength of 0.81 and in two satellite lines at 41.95 and 45.15 eV ionization energy with pole strengths of 0.06 and 0.02, respectively. Similarly, the $2\sigma_u$ ionization leads to the appearance of a ''main'' line at 39.09 eV with a pole strength of 0.79 accompanied by two satellite lines at 41.95 and 45.16 eV possessing the pole strengths of 0.07 and 0.02, respectively. The less pronounced satellite structure and the absence of the breakdown of the orbital picture of ionization predicted for this molecule is partly due to the smaller number of electrons.

To make a simple characterization of the computed main and satellite ionic states for BeF_4^{2-}, BeF_3^-, and BeF_2 we recall the peculiar spatial electron distribution present in these systems. As has been discussed in Ref. 52 the bonding in these systems, in particular in the dianion, is highly ionic with the outer-valence electron density predominantly residing on the symmetry equivalent fluorine ligands and the central beryllium atom being positively charged. Therefore, we may expect the vacancies created upon ionization and excitation to be essentially localized on the fluorine sites. The virtual orbitals are somewhat more difficult to characterize since these orbitals represent—apart from a few exceptions—admixtures of components deriving from both the fluorine ligands and the central beryllium atom. However, as a closer analysis reveals, the metallic character of almost all of these orbitals is obvious.

Owing to the above characterization of the orbitals and the localization of the electronic charge density we may denote the single-hole configurations corresponding to the outer-valence orbitals as $F2p^{-1}$ which simply implies that the hole created upon ionization is essentially localized on one of the fluorine atoms. The $2h1p$ configurations associated with the satellite states may be divided into two groups which we collectively denote as $F2p^{-1}\ F'2p^{-1}\ M'^{+}$ and $F2p^{-2}\ M'^{+}$. The $F2p^{-1}\ F'2p^{-1}\ M'^{+}$ configuration indicates that one electron is excited from one of the fluorine ligands to the central beryllium upon ionization of a further electron which stems from a fluorine atom other than the excited one (''two-site configuration''). Likewise, the $F2p^{-2}\ M'^{+}$ con-

figuration implies that both the ionized and excited electrons stem from the same fluorine atom (''one-site configuration''). Physically, the above $2h1p$ configurations describe a charge transfer of negative charge from fluorine to the central, almost positive, beryllium. The increasing many-body effects in the inner-valence energy region when going from BeF_2 to BeF_4^{2-} is related to the growing ionicity and hence to the growing efficiency of the charge transfer in these systems.

VII. CONCLUSIONS AND OUTLOOK

In the present work we have discussed the relevance of the block or band Lanczos method for calculating the one-particle Green's function. The usual way for determining this function is to resort to the Dyson equation whose solution reduces to the diagonalization of large-dimensional Hermitian secular matrices. We have shown that the block Lanczos method quite naturally applies to the emerging secular problems allowing for their efficient computation.

To make transparent the importance of the block Lanczos method within the one-particle Green's function framework we recall that its applicability heavily depends on the specific structure of the secular problem. As we have pointed out, in the secular matrix (Dyson equation) to be diagonalized a block of small dimension (the $1p/1h$ block) is coupled to two larger blocks which do not couple with each other. Without loss of generality we have explicitly discussed the ADC(3) Dyson equation as a specific example. There, the latter two blocks are the $2p1h$ and $2h1p$ blocks. Based on the major prerequisite that the $2p1h$ and $2h1p$ blocks can be treated independently and that the $2p1h$ block is energetically well separated from the $2h1p$ block and thus has minor influence on the cationic solutions being sought, we have transformed the *very large* $2p1h$ block using block Lanczos. In this way a rather reliable approximation of the $2p1h$ block in the region of ionization is obtained. As a result the dimension of the secular matrix which is subject to subsequent diagonalization is substantially reduced.

The computational performance of the proposed procedure has been tested in calculating the vertical ionization energies and accompanying spectral intensity coefficients of the valence ionic states in benzene. The approximate values of these quantities obtained by the prediagonalized Dyson equation have been compared to the corresponding ''exact'' values of the full secular problem. The results for the valence ionic states of $^2E_{2g}$ and $^2A_{1g}$ symmetry have been discussed in detail. It has been demonstrated that a rather crude pseudospectrum of the $2p1h$ block already suffices to reproduce all the valence ionic levels to a sufficient degree of accuracy. The results further show the expected tendency of a faster convergence of the outer-valence states than is observed for the inner-valence states.

As a further model application of the procedure we have calculated the valence-shell ionization spectra of BeF_4^{2-}, BeF_3^-, and BeF_2 using the ADC(3) Green's function approach. The diagonalization of the secular matrices arising for the BeF_4^{2-} and BeF_3^- systems has proven to be a particular delicate problem in view of the large number of closely lying states to be determined in the inner-valence regime of their ionization spectra. Here, the block Lanczos transformation has substantially reduced the computational effort as one has now to cope with smaller secular matrices. We have discussed the electronic structure of the computed spectral profiles of the above beryllium fluorides in relation to the peculiar bonding properties present in these systems.

The efficiency of applying the block Lanczos prediagonalization grows, on the one hand, with the size of the configuration spaces defining the dimension of the secular matrices to be diagonalized and, on the other hand, with the number of roots being sought. As we have pointed out, the dimension of the secular problem is substantially determined by the size of the $2h1p$ block and, in particular, by that of the $2p1h$ block. For a molecule under consideration the size of the configuration spaces of these blocks crucially depends on the orbital basis set employed, i.e., on the number of occupied and unoccupied (virtual) orbitals. Enlarging the basis set the $2p1h$ block grows much faster with the basis set than does the $2h1p$ block, hence facilitating the application of the block Lanczos prediagonalization. The second important aspect concerns the number of eigensolutions wanted. As far as one is only interested in a few selected roots, e.g., in those corresponding to the outer-valence ionic states of a molecule one may directly apply the block Davidson diagonalization procedure (or any other proper diagonalization method) to generate the desired information from the secular matrix. Considerable numerical difficulties, however, arise when a multitude of solutions is required. In this situation, especially when the density of cationic states is large, the block Lanczos prediagonalization is advantageous.

The success in the ADC(3) applications for the one-particle Green's function renders the block Lanczos method also a promising method for the treatment of the next higher level of approximation, the fourth-order scheme, ADC(4). From the numerical point of view the ADC(4) approximation poses two major bottlenecks. One drawback opposing actual applications is the calculation of special effective matrix elements involving sums of Coulomb interactions running over four one-particle quantum numbers. The other difficulty originates from the size of the configuration spaces. In the ADC(4) scheme, the next higher class of excitations, i.e., $3p2h$ and $3h2p$ excitations is explicitly introduced leading to secular matrices whose dimensions surmount those of the ADC(3) scheme considerably. The essential mathematical procedures now involve the diagonalization of Hermitian secular matrices built up of the blocks $1p/1h$, $2p1h/3p2h$, and $2h1p/3h2p$, where the $3h2p$ block and, in particular, the $3p2h$ block are very large. Here, we expect that the block Lanczos prediagonalization will be extremely advantageous in order to cope with the otherwise very demanding full ADC(4) matrices.

Finally, we briefly outline a further application of the block Lanczos method within the many-body Green's function framework. This application aims at the computation of the particle–particle (p–p) propagator which is a component of the two-particle Green's function. The p–p propagator

bears direct access to the energies and accompanying spectral transitions of doubly ionized states in molecules. The ADC(2) expansion of the spectral representation of the p−p propagator leads to an eigenvalue problem in the space of two-hole and three-hole one-particle configurations defined with respect to the N-electron HF orbital basis. In practical applications one often has to compute a multitude of states (typically several hundreds) which obviously represents a formidable task. On the other hand, it is useless to determine all the states from the high-dimensional secular matrices since the individual states cannot usually be resolved in the experiment. In order to simulate the spectral profile of the spectrum it is, therefore, reasonable only to reproduce its collective or general features. In this respect the block Lanczos method should prove to be a powerful tool in view of the global convergence properties which it does account for.

ACKNOWLEDGMENT

Financial support by the Deutsche Forschungsgemeinschaft is acknowledged.

[1] A. A. Abrikosov, L. P. Gorkov, and I. E. Dzyaloshinski, *Methods of Quantum Field Theory in Statistical Physics* (Prentice-Hall, Englewood Cliffs, 1963).
[2] A. B. Migdal, *Theory of Finite Fermi Systems* (Wiley-Interscience, New York, 1967).
[3] R. D. Mattuck, *A Guide to Feynman Diagrams in the Many-Body Problem* (McGraw-Hill, New York, 1967).
[4] A. L. Fetter, and J. D. Walecka, *Quantum Theory of Many-Particle Systems* (McGraw-Hill, New York, 1971).
[5] C. Lanczos, J. Res. Natl. Bur. Stand. **45**, 255 (1950).
[6] B. N. Parlett, *The Symmetric Eigenvalue Problem* (Prentice-Hall, Englewood Cliffs, 1980).
[7] J. K. Cullum and R. A. Willoughby, *Lanczos Algorithms for Large Symmetric Eigenvalue Computations* (Birkhäuser, Boston, 1985).
[8] A. Ruhe, Math. Comput. **33**, 680 (1979).
[9] C. M. M. Nex, Comput. Phys. Commun. **53**, 141 (1989).
[10] H.-D. Meyer and S. Pal, J. Chem. Phys. **91**, 6195 (1989).
[11] Y. V. Vorobyev, *Method of Moments in Applied Mathematics* (Gordon and Breach, New York, 1965).
[12] N. I. Akhiezer, *The Classical Moment Problem*, (Oliver and Boyd, London, 1965).
[13] L. S. Cederbaum, Mol. Phys. **28**, 479 (1974).
[14] L. S. Cederbaum and W. Domcke, Adv. Chem. Phys. **36**, 205 (1977).
[15] L. S. Cederbaum, W. Domcke, J. Schirmer, and W. von Niessen, Adv. Chem. Phys. **65**, 115 (1986).
[16] S. Ethofer and P. Schuck, Z. Phys. **228**, 264 (1969).
[17] J. Winter, Nucl. Phys. A **194**, 535 (1972).
[18] L. S. Cederbaum, J. Chem. Phys. **62**, 2160 (1975).
[19] L. S. Cederbaum, W. Domcke, J. Schirmer, W. von Niessen, G. H. F. Diercksen, and W. P. Kraemer, J. Chem. Phys. **69**, 1591 (1978).
[20] J. Schirmer, Phys. Rev. A **26**, 2395 (1982).
[21] J. Schirmer, L. S. Cederbaum, and O. Walter, Phys. Rev. A **28**, 1237 (1983).
[22] J. Schirmer and A. Barth, Z. Phys. A **317**, 267 (1984).
[23] A. Tarantelli and L. S. Cederbaum, Phys. Rev. A **39**, 1656 (1989).
[24] A. Tarantelli and L. S. Cederbaum, Phys. Rev. A **46**, 81 (1992).
[25] J. H. Wilkinson, *The Algebraic Eigenvalue Problem* (Oxford University, New York, 1965).
[26] G. Moro and J. H. Freed, J. Chem. Phys. **74**, 3757 (1981).
[27] E. Haller, L. S. Cederbaum, and W. Domcke, Mol. Phys. **41**, 1291 (1980).
[28] H. Köppel, W. Domcke, and L. S. Cederbaum, Adv. Chem. Phys. **57**, 59 (1984).
[29] A. Nauts and R. E. Wyatt, Phys. Rev. Lett. **51**, 2238 (1983).
[30] R. E. Wyatt, Chem. Phys. Lett. **121**, 301 (1985).
[31] C. Duneczky, R. E. Wyatt, D. Chatfield, K. Haug, D. W. Schwenke, D. G. Truhlar, Y. Sun, and D. J. Kouri, Comput. Phys. Commun. **53**, 357 (1989).
[32] T. J. Gil, C. L. Winstead, and P. W. Langhoff, Comput. Phys. Commun. **53**, 123 (1989).
[33] N. Ben-Tal and N. Moiseyev, J. Phys. A **24**, 3593 (1991).
[34] E. R. Davidson, J. Comput. Phys. **17**, 87 (1975).
[35] W. Butscher and W. E. Kammer, J. Comput. Phys. **20**, 313 (1976).
[36] B. Liu, in *Numerical Algorithms in Chemistry: Algebraic Methods*, LBL-8158 (Lawrence Berkeley Laboratory, 1978).
[37] F. Tarantelli (unpublished, 1985).
[38] F. Tarantelli, A. Sgamellotti, L. S. Cederbaum, and J. Schirmer, J. Chem. Phys. **86**, 2201 (1987).
[39] C. W. Murray, S. C. Racine, and E. R. Davidson, J. Comput. Phys. **103**, 382 (1992).
[40] D. K. Faddeev and V. N. Faddeeva, *Computational Methods of Linear Algebra* (Freeman, San Francisco, 1963).
[41] W. von Niessen, J. Schirmer, and L. S. Cederbaum, Comput. Phys. Rep. **1**, 57 (1984).
[42] O. Walter, L. S. Cederbaum, and J. Schirmer, J. Math. Phys. **25**, 729 (1984)
[43] J. Schirmer and G. Angonoa, J. Chem. Phys. **91**, 1754 (1989). .
[44] F. B. Hildebrand, *Introduction to Numerical Analysis* (McGraw-Hill, New York, 1974).
[45] The computer program used is based on the original version written by O. Walter and G. Angonoa in Heidelberg.
[46] G. Herzberg, *Electronic Spectra of Polyatomic Molecules* (Van Nostrand, Princeton, 1966).
[47] S. Huzinaga, J. Chem. Phys. **42**, 1293 (1965).
[48] T. H. Dunning, J. Chem. Phys. **53**, 2823 (1970).
[49] H.-G. Weikert and L. S. Cederbaum, Chem. Phys. Lett. **237**, 1 (1995).
[50] T. H. Dunning, J. Chem. Phys. **55**, 716 (1971).
[51] H.-G. Weikert, L. S. Cederbaum, F. Tarantelli, and A. I. Boldyrev, Z. Phys. D **18**, 299 (1991).
[52] H.-G. Weikert and L. S. Cederbaum, J. Chem. Phys. **99**, 8877 (1993).
[53] H.-G. Weikert, Thesis, Universität Heidelberg, 1993.